Magnetic and Scaling Properties of $YBa_2Cu_4O_8$ High-Temperature Superconductor

by

Fuad Mohammed Fayez Enaya

A Thesis Presented to the

FACULTY OF THE COLLEGE OF GRADUATE STUDIES

KING FAHD UNIVERSITY OF PETROLEUM & MINERALS

DHAHRAN, SAUDI ARABIA

In Partial Fulfillment of the
Requirements for the Degree of

MASTER OF SCIENCE

In

PHYSICS

October, 1998

INFORMATION TO USERS

This manuscript has been reproduced from the microfilm master. UMI films the text directly from the original or copy submitted. Thus, some thesis and dissertation copies are in typewriter face, while others may be from any type of computer printer.

The quality of this reproduction is dependent upon the quality of the copy submitted. Broken or indistinct print, colored or poor quality illustrations and photographs, print bleedthrough, substandard margins, and improper alignment can adversely affect reproduction.

In the unlikely event that the author did not send UMI a complete manuscript and there are missing pages, these will be noted. Also, if unauthorized copyright material had to be removed, a note will indicate the deletion.

Oversize materials (e.g., maps, drawings, charts) are reproduced by sectioning the original, beginning at the upper left-hand corner and continuing from left to right in equal sections with small overlaps. Each original is also photographed in one exposure and is included in reduced form at the back of the book.

Photographs included in the original manuscript have been reproduced xerographically in this copy. Higher quality 6" x 9" black and white photographic prints are available for any photographs or illustrations appearing in this copy for an additional charge. Contact UMI directly to order.

UMI

A Bell & Howell Information Company
300 North Zeeb Road, Ann Arbor MI 48106-1346 USA
313/761-4700 800/521-0600

Magnetic and Scaling Properties of $YBa_2Cu_4O_8$ High-Temperature Superconductor

BY

Fuad Mohammed Fayez Enaya

A Thesis Presented to the

FACULTY OF THE COLLEGE OF GRADUATE STUDIES

KING FAHD UNIVERSITY OF PETROLEUM & MINERALS

DHAHRAN, SAUDI ARABIA

In Partial Fulfillment of the
Requirements for the Degree of

MASTER OF SCIENCE

In

PHYSICS

OCTOBER 1998

UMI
300 North Zeeb Road
Ann Arbor, MI 48103

KING FAHD UNIVERSITY OF PETROLEUM AND MINERALS
DHAHRAN 31261, SAUDI ARABIA
COLLEGE OF GRADUATE STUDIES

This thesis, written by Fuad Mohammed Enaya under the direction of his Thesis Advisor and approved by his Thesis Committee, has been presented to and accepted by the Dean of the College of Graduate Studies, in partial fulfillment of the requirements for the degree of **MASTER OF SCIENCE in PHYSICS**

Thesis Committee:

Dr. Khalil A. Ziq
(Chairman)

Dr. N. M. Hamdan
(Member)

Dr. A. S. Al-Harthi
(Member)

Dr. J. Shirokoff
(Member)

Dr. N. Tabet
(Member)

Dr. Mahmoud Al-Nagadi
(Department Chairman)

Dr. Abdullah Al-Shehri
Dean, College of Graduate Studies

Date

Dedication

To

my Parents, my Wife,

my Brothers, my Sisters

and my children " Mohammed and Farah "

with Love and Gratitude

ABSTRACT

Magnetic studies on polycrystal $YBa_2Cu_4O_8$ High-T_c ceramic, through its hysteresis loops, reveals that the remanent magnetization initially increases rapidly, while increasing the field, then approaches saturation gradually at high field. The magnetic energy losses are increasing with field while the increases of the temperature reduces the energy loss inside the sample. Moreover, the critical current density is also decreased with field up to certain field where it becomes almost field independent. Pinning force at a given temperature, initially increases linearly with field then at high field it increases gradually with smaller (saturation) slope.

Upon studying the scaling behavior of the superconducting state properties, two methods were followed. The common method, where two different scaling parameters were used and the scaling plots are achieved -particularly at high temperature and high field- as revealed by universal behavior of the represented superconducting properties. A new scaling model is presented in this thesis and applied for various superconducting properties. The model is based on one scaling parameter and can be applied over a wide range of temperatures. The scaling parameter deduced from the pinning force represents a sort of threshold field above which the pinning force gradually approaches saturation or maximum.

خلاصة الرسالة

تم قياس تغير الخصائص المغناطيسية لعينة ($Yba_2Cu_4O_8$) من خلال تأثير مجالات مغناطيسية مختلفة عند درجات حرارة مختلفة بهدف دراسة الطاقة المفقودة والمغناطيسية المتبقية وسلوك التيارات الحرجة والقوى المثبتة داخل العينة. وجد من خلال الدراسة أن الطاقة المفقودة تتزايد مع ازدياد المحال المغناطيسي كما تتناقص هذه الطاقة المفقودة بارتفاع درجة الحرارة أثناء التجربة. هذا وكان سلوك المغناطيسية المتبقية مماثلاً لسلوك الطاقة المفقودة مع تغير المجال المغناطيسي ودرجة الحرارة. ووجد كذلك أن كثافة التيارات الحرجة تتناقص بتزايد المجال المغناطيسي إلى حد معين، تصبح بعدها هذه التيارات قليلة التأثر بتزايد قيمة المجال المغناطيسي. أما بالنسبة للقوى المثبتة –عند درجة حرارة معينة– فإنها تتزايد مبدئياً بشكل خطي بتزايد المجال المغناطيسي ثم بوصول المجال المغناطيسي لقيمة عالية يبدأ معدل ازدياد القوى المثبتة بالتناقص التدريجي البطيء حتى تصل لمرحلة الثبات الخطي.

فضلاً على ذلك فقد تم من خلال هذه الأطروحة دراسة سلوك المعايرة للخصائص المغناطيسية لنفس العينة من خلال طريقتين. أولاهما هي الطريقة الشائع اتباعها من خلال إجراء المعايرة بواسطة عاملين للمعايرة أو أكثر، وكانت نتائج المعايرة في أفضل صورها بالنسبة للحالات التي تمت عند درجات حرارة مرتفعة وعند وجود مجالات مغناطيسية عالية. أما الطريقة الأخرى فهي النموذج المطور للمعايرة – والذي نعرضه في هذه الأطروحة لأول مرة– من خلال استخدام عامل معايرة وحيد، بحيث يتم استعماله على نطاق واسع من درجات الحرارة، وهذه الطريقة –أيضاً– أعطت نتائج جيدة لسلوك المعايرة خاصة للقوى المثبتة والتيارات الحرجة.

يمثل معامل المعايرة هذا – والذي حصلنا عليه من منحنيات القوى المثبتة – نوعاً من مجالات الانطلاق والتي بعدها تصل القوى المثبتة تدريجيا إلى قيمة قصوى أو إلى حالة الإشباع.

Acknowledgement

All my thanks to "ALLAH" for giving me patient that enabled me to accomplish this project successfully.

I would like to express my sincere indebtedness and gratitude to my supervisor Dr. Khalil A. Ziq for his lively interest, guidance and encouragement throughout this research.

I would like also to thank my thesis committee: Dr. N. Hamdan, Dr. A. Al-Harthi, Dr. J. Shirokoff and Dr. N. Tabet for their countless discussions and valuable suggestions and interest.

Thanks are also due to members of the physics. Each has contributed positively in his own way specially Dr. A. Aswad, Dr. O. Dabbousi, Dr. A. Mekki and Mr. M. Abdulhadi for the moral support and valued suggestions.

Many thanks are due to KFUPM SCHOOLS (administration and colleagues) for their everlasting support during my study at the university.

My deep thanks to Dr. R. Ramadan for his general interest and advice during various stages of my study at KFUPM.

The contribution of my wife towards the completion of this work is limitless. I would like also to thank all my family members, relatives and neighbors for their warm feelings during my studying period.

Finally I am grateful to King Fahad University of Petroleum and Minerals for the productive atmosphere that allowed me to complete this research.

Contents

List of Figures

List of Tables

CHAPTER 1

Introduction

1.1 Historical Background

Superconducting materials exhibit a remarkable combination of electric and magnetic properties which appear only when cooled to extremely low temperatures [1].

Low temperature experimental investigations were first made possible when Kamerlengh Onnes liquefied helium in 1908, [2]. Three years later, the Onnes investigation team discovered superconductivity while measuring the resistivity of elemental mercury. They observed a sharp drop in the resistance of mercury down to "zero" at about 4.2K. At this temperature, known as the critical temperature (T_c), the specimen undergoes a phase transition from a state of normal electrical resistivity to a state of zero resistance, Onnes coined the term Superconductor [3].

In 1933, the second characterizing property, "perfect diamagnetism", was discovered by Meissner and Oschsenfeld [4]. When a superconductor (SC) sample is subjected to an applied magnetic field, then cooled to temperatures below the critical temperature ($T < T_c$), the magnetic flux is expelled out of the sample interior as long as the

applied field is below a known critical field H_c. This is called the Meissner effect and it can be seen in figure 1.1a [4].

1.2 Types of Superconductors

Superconductors are generally divided into two types: type-I and type-II depending on their behavior in an applied magnetic field.

The magnetization curve expected for a superconductor (SC) under the conditions of the Meissner effect is shown in figure 1.1a. Note that the initial slope of the magnetization while increasing the field is negative because of the diamagnetism, with a slope = $-1/4\pi$ for perfect shielding. Pure superconducting specimens of many elemental materials exhibit this behavior and they are called type-I superconductors or, formerly, soft superconductors. As seen in figure 1.1a there is a critical field H_c, below which the material is in superconducting state and above it the material becomes a normal conductor. It is of practical importance to determine the value of H_c that separate the two regions, and marks the transition between superconducting and normal state. The critical field is related to the critical temperature by Tuyn's empirical formula [2]. A result which is readily obtained from the Gorter and Casimir phenomenological two fluid model.

The values of the critical field, H_c are usually too low for type-I super conductors to have any useful technical application as for example, in coils for superconducting magnets [4]. In figure 1.1, a schematic representation of the reversible magnetization is shown. In the absence of pinning centers, the magnetization is ideal or reversible.

Other materials exhibit a magnetization curve of the form shown in figure 1.1b and are known as type-II super conductors. Conventional type-II SC are commonly alloys or transition metals elements (like Nb,V and Ta) with relatively high values of the electrical resistivity in the normal state compared to Cu, for example. Newly discovered SC materials are ceramic oxides.

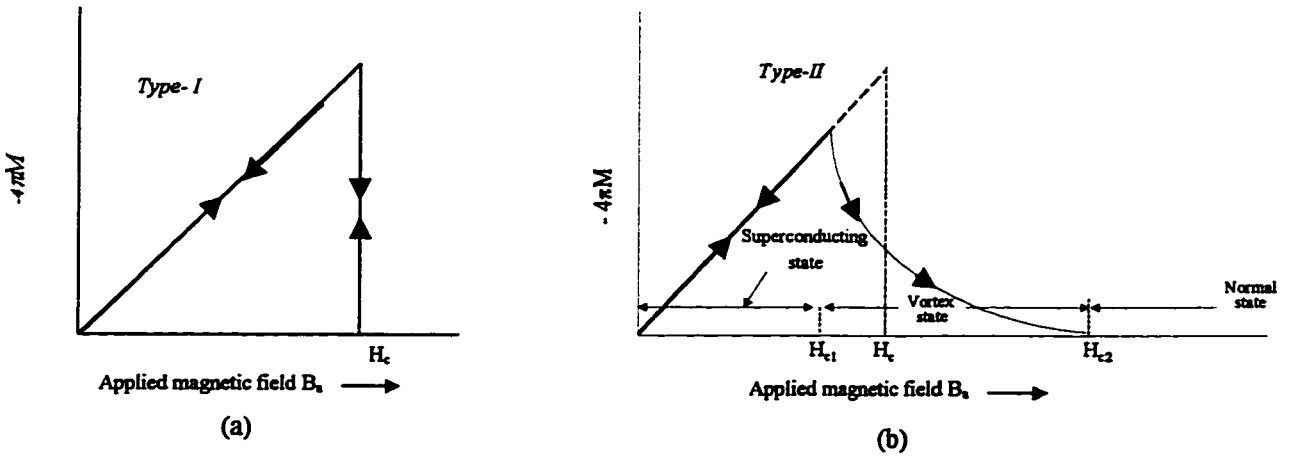

Figure: 1.1

(a): magnetization versus applied magnetic field for a superconductor of type-I.

(b) superconducting magnetization curve of type-II superconductors.

In type-II SC, the flux starts penetrating the material in selected regions (vortices) at a field H_{c1} known as (the lower critical field). At higher fields, flux penetration increases, and the density of vortices increases, and flux penetration completely penetrates the specimen, destroying the superconducting state at an upper critical field H_{c2}. Between the lower critical field H_{c1} and the upper critical field H_{c2} the flux density $B \neq 0$ and the Meissner effect is said to be incomplete or mixed state. Above H_{c2} the material is a normal conductor and below H_{c1} the material is a superconductor. In general, for the same material, the value of H_{c2} can reach as high as 100 times or more than the value of the critical field H_{c1} calculated from the thermodynamics of the transition. In the region between H_{c1} and H_{c2} the SC is threaded by flux lines and is said to be in the vortex state [4].

The ideal (reversible) magnetic behavior of type-II SC was investigated theoretically by Alexi Abrikosov [5]. He proposed that in the case of the applied field above H_{c1}, bundles of magnetic flux lines penetrate the SC but still allow current to flow on either side. As the applied field increase to H_{c2}, the number of bundles, or vortices increase. The magnetic field "lines" generated become more densely packed throughout the SC until the field bundles finally overlap and destroy superconductivity. For fields above H_{c2}, the material returns to its normal state [5,6].

The area under the reversible thermodynamical magnetization represent the condensation energy which is given as = $H_c^2/8\pi$. For a given H_c the area under the magnetization curve, for type-II, is the same as for type-I.

One of the properties of SC is their ***"energy gap"***. This energy gap of superconductors is different than the energy gap in insulators. In insulators the energy gap is tied to the lattice, while for superconductors the gap is tied to the superconducting state

itself. Also from experimental data it is established that the exponential in the heat capacity is known to be one-half of the energy gap [4].

The transition in zero magnetic field from the superconducting state to the normal state is observed to be a second-order phase transition. At a second-order transition there is no latent heat, but there is a discontinuity in the heat capacity. Further, the energy gap decreases continuously to zero as the temperature is increased to the transition temperature T_c [4].

1.3 High Temperature Superconductors

In 1986, Bednorz and Müller made a remarkable contribution to the SC field [7]. They discovered a new superconducting material with transition temperature higher than had been thought possible. This new generation of superconductors is based on ceramic oxides that have high transition temperature (high T_c), nearly 35K, for metallic compound of (Ba-La-Cu-O). Previously, the highest superconducting transition temperature (T_c) for conventional SC-II was 23.3K for Nb_3Ge [8]. This marked the beginning of a new era of High Temperature Superconductivity (HTSC) [7].

The main HTSC family grouped as follows:

- Yttrium based copper oxide ($YBa_2Cu_3O_{7+\delta}$) with a T_c of about 93K was discovered in 1987 by Chu *et al* [9]. This group of HTSC was widely studied since it was the first superconductor with a transition temperature higher than the boiling point of liquid nitrogen. Apart from its easy preparation, it has a very high H_{c2}. However, its critical current (J_c) at 4.2K is lower than that for Nb-compound, a conventional SC-II [9].

- Bismuth based copper oxide (Bi-Ca-Sr-Cu-O) with T_c about 110K (for Bi-2223), discovered by Maeda and co-worker in 1988 [10].

- Thallium based copper oxide (Ti-Ca-Ba-Cu-O) with T_c about 125K (for Tl-2223), found in 1988 by Hermann and Sheng [11-12].

- Mercury based copper oxide (Hg-Ba-Ca-Cu-O) with T_c about 135K, found in 1993 [13].

There are some differences and similarities between conventional superconductors and HTSC. In HTSC, the structure is strongly anisotropic with a very large Ginzburg-Landau (GL) parameter, ($\kappa = \lambda/\xi$) where λ is the penetration depth and ξ is the coherence length. This is due to the small value of $\xi \sim 10$ μm. The crystalline structure reflects the different anisotropic superconducting properties along the crystal directions. The upper critical field is very high in HTSC ~ 100 Tesla, while the critical current density is relatively small compared to the critical current density in conventional superconductors (even at 4.2K).

Also, the transition temperature of HTSC is sensitive to the amount of oxygen content in the sample [14, 12]. Other similarities that exist within conventional superconductor are the energy gap, Josephson-Tunneling, and discontinuity in specific heat.

1.4 Field Cooled and Zero Field Cooled States

As a consequence of Meissner effect, the magnetic state of superconducting material depends on the history of the state. In particular: Field Cooled (FC) and Zero Field Cooled (ZFC) states. In the FC mode, the magnetic field (H_{cool}) is applied at $T > T_c$. The sample is then cooled down to a measurement temperature $T_m > T_c$. While for ZFC mode, no field is applied at $T > T_c$. The sample is then cooled down to $T_m < T_c$. Magnetic and transport properties of these two states are in general very different.

Since flux is initially absent from the sample during ZFC, the observed diamagnetism after applying a field represents flux exclusion from the sample. In contrast to the ZFC case, for the FC state a flux is generally uniformly present in the sample above T_c. Therefore, any diamagnetic moment M_{Fc} which appears as a result of field-cooling represents a flux expulsion, often referred to as the Meissner effect [15].

1.5 Review of Scaling

Several methods were applied to scale the SC properties. Kramer scaled the pinning force, at temperatures near T_c, using two scaling parameters, maximum pinning force $F_{p(max)}$ and upper critical field H_{c2} [16]. The same method has been followed for

different SC by Juang *et al.* [17]. Chang *et al.* also did the scaling of pinning force using two scaling parameters, $F_{p(max)}$ and H_{irr} (irreversible field at which pinning force goes to zero) [18]. Wei *et al.* followed "Kramer's" method in scaling pinning force using H* instead of H_2, where H* is the field where F_p vanishes [19]. Song *et al.* used $F_{p(max)}$, H_{irr}, H* in scaling procedure [20]. Wolfus *et al.* used two scaling parameters to scale the magnetization variation with field at different temperatures. These parameters are H_m and M_m, where H_m is the field where M reaches its minimum value M_m [21].

The importance of scaling could be illustrated as follows: If one needs to measure, for example, the pinning force at certain temperature and field, then the behavior of F_p with field at any temperature can be predicted. One can also obtain useful information about superconducting properties for the cases where experimental conditions are not favorable [22].

1.6 Statement of the Problem and Motivation

In this thesis, magnetic measurements are reported on a YBa_2Cu-high T_c superconductor. In particular, magnetic energy loss, remanent magnetization, critical current density and pinning forces for two states, ZFC and FC are studied. Moreover scaling of these properties will be extensively studied.

Since the magnetic properties of these latter two states are different, one expects that many related properties are also different. For example, magnetic energy loss, pinning forces, remanent magnetization and critical current density .

The area of the hysteresis loops, evaluated by integrating the area under the magnetization curve, represents magnetic energy loss in the sample as a result of cycling the field between two maxima. This area depends on the magnetic state, maximum of the cycling magnetic field and the temperature [15,23,24].

Y-based superconductors are relatively easy to prepare and have many interesting properties like for example, strong pinning force, that have been widely studied. There are two main subgroups in the Y-basis: $YBa_2Cu_3O_7$ (Y_{123}) and $YBa_2Cu_4O_8$ (Y_{124}), where the numbers (123) and (124) indicates the number of Y,Ba and Cu atoms in the superconducting material.

The objectives in this research are:

- To study the variations of remanent magnetization, energy losses with field and temperature and how they can be related to the scaling properties of the hysteresis loops for FC and ZFC states in Y_{124}.
- To obtain the critical current density and pinning forces for different regions of field and temperature for FC and ZFC states in Y_{124} and to study the scaling behavior of these quantities.

CHAPTER 2

Experimental

2.1 Sample Preparation

A solid state reaction method has been used to first prepare polycrystalline $Y_1Ba_2Cu_3O_7$ which is used to prepare $Y_1Ba_2Cu_4O_8$. Stoichiometric ratio of Y : Ba : Cu = 1 : 2 : 3 using high purity (99,999%) powder of (Y_2O_3), ($BaCu_3$) and (CuO) were mixed thoroughly by grinding for about a half an hour. The mixture was then placed in an alumina crucible and furnace for calcination in air at 890 °C for about 18 hr. During the calcination process, carbon is released from $BaCO_3$ as CO_2. After cooling, the sample is re-ground for about 30 minutes and the calcination process was repeated three times. Then the resultant mixture was re-ground and pressed to form 2-3 mm thick by 10-13 mm diameter pellets at a pressure of 3000 kg/cm^2. Finally, the pellets are sintered in oxygen atmosphere at a temperature of 950 °C for 6 hr [25].

An appropriate amount of copper oxide (CuO) was then added to $Y_1Ba_2Cu_4O_7$ to yield $Y_1Ba_2Cu_4O_8$:

$$Y_1Ba_2Cu_3O_7 + CuO \rightarrow Y_1Ba_2Cu_4O_8$$

Again the resultant mixture was ground and pressed into 2-3 mm thick by 10-13 mm diameter pellets at a pressure of about 4000 kg/cm^2 and annealed at 950 °C in oxygen atmosphere for 6hr. The annealed pellet was further re-grounded, pelletized under the same conditions and the annealing procedure was repeated for at least three times. Furnace cooling was used throughout the preparation process.

2.2 Experimental Technique

Magnetic properties are studied using a computer controlled PAR-Lakeshore 4500/150A variable temperature vibrating sample magnetometer (VSM) system. It combines a VSM with a high field superconducting solenoid generating magnetic field up to 9 Tesla and a variable temperature cryostat in the range of 1.8 to 300K.

The VSM system consists of the following major parts :

1. Vibrating head and sample holder.
2. Variable temperature cryostat.
3. Temperature controller.
4. VSM controller.
5. Power supply and controller.
6. Personal computer (PC) with a National Instrument IEEE-488 GPIB-PcII connected to all controllers.

For more detailed information about the system setup see reference [23].

2.3 Sample Characterization

The superconducting transition temperature, T_c, has been measured using two ways:

- Four-Point Probe method (R vs. T) with passing current (I= 5mA). Tc was found to be about 82K, see figure 2.1.
- Finding T_c from the variation of remanent magnetization M_r with temperature T, where M_r goes to zero at T_c. The result was found to be close to the previous method, Tc about 82K, see figure 2.2.

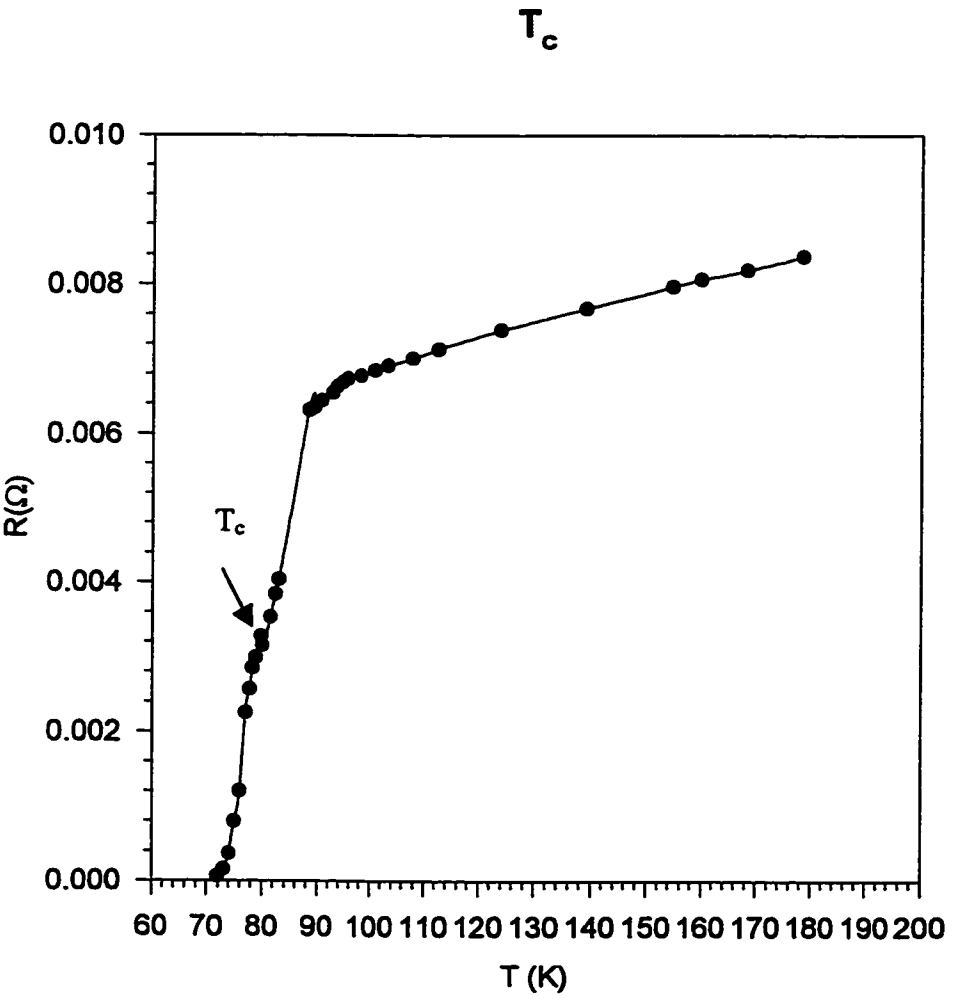

Figure 2.1: Resistance dependence with temperature of Y_{124}.

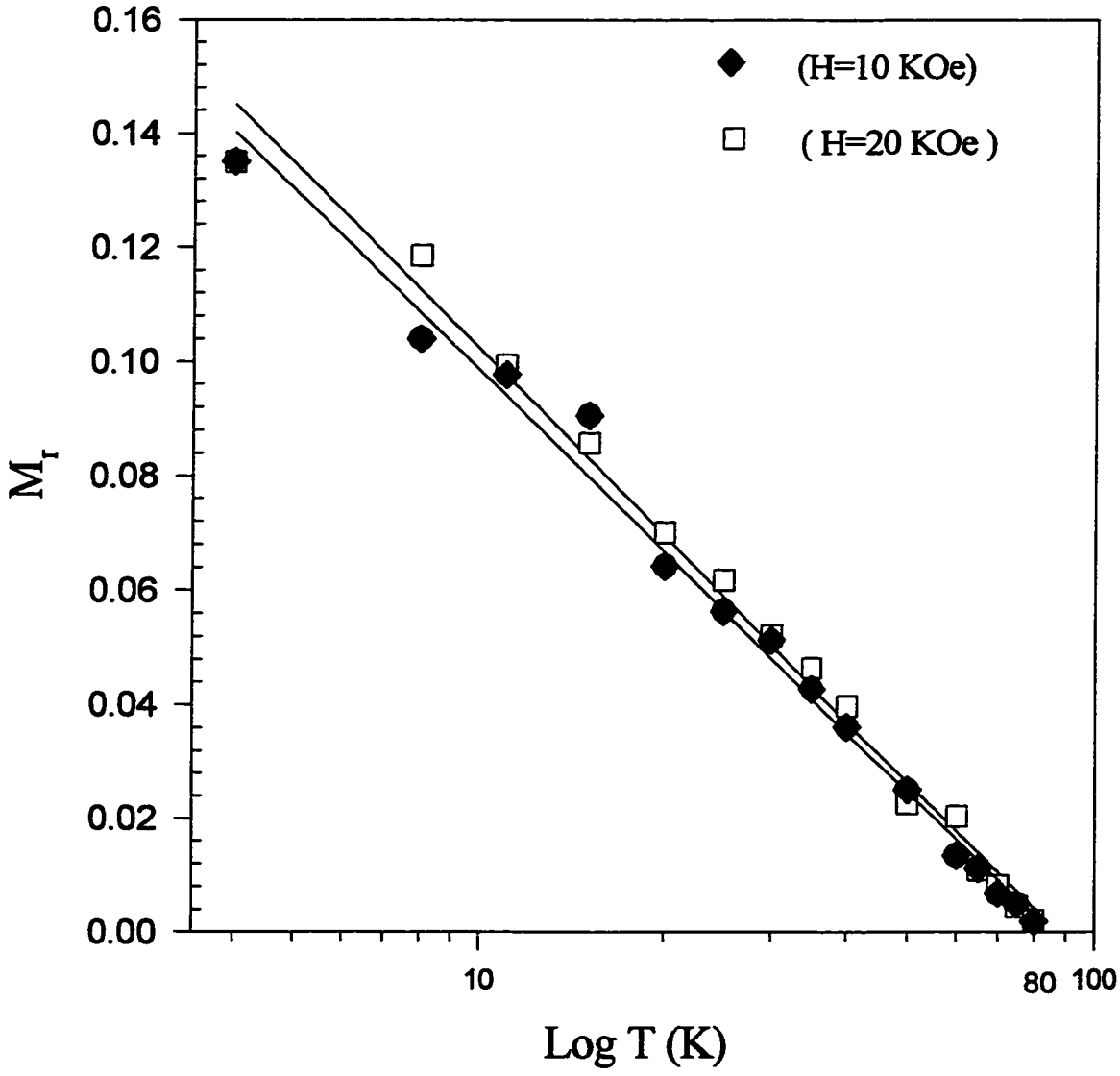

Figure 2.2: M_r dependence with temperature of Y_{124} at two selected fields 10 and 20 kOe.(*semi-log scale*)

X-Ray Diffraction (XRD):

An X-ray diffraction pattern was measured for the Y_{124} sample to find out its lattice parameters (a, b, c), see figure2.3. The results are listed in table 2.1 they are consistent with other published results in the literature [26]. The XRD pattern was obtained using a Philips PW1700 XRD employing a Cu X-ray tube operating at 40 kV and 30 mA.

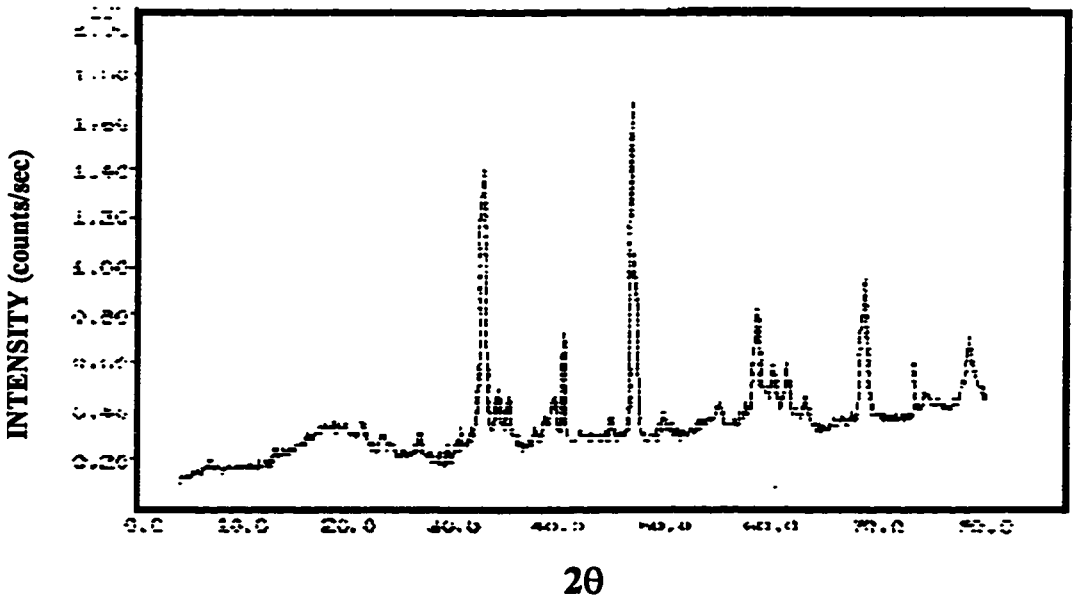

Figure 2.3 : X-ray diffraction pattern of Y_{124}.

Table. 2.1

X-ray lattice parameters for Y_{124}.

XRD	a(Å)	b(Å)	c(Å)	Volume $(Å)^3$	a/b	c/b
Our Results	3.83943	3.87042	27.1889	404.03	0.992	7.025
Published Results	3.8413	3.8711	27.239	405.04	0.992	7.036

CHAPTER 3

Remanent Magnetization and Scaling of Hysteresis Loops

3.1 Introduction

The superconducting state of any "non-ideal" superconducting material depends on the history in which the state is being prepared. Analogous to spin-glass materials, when a superconductor is cooled in zero field (ZFC) from above its transition temperature, flux is absent from the sample at the measuring temperature. In this state, the observed diamagnetism after applying a magnetic field represents flux exclusion from the sample. When a magnetic field, higher than the lower critical field H_{c1}, is applied to a type-II SC, the magnetic flux then penetrates into the bulk of the sample. In the presence of defects such as pinning centers, some of the flux lines remain trapped within the bulk showing a positive magnetic moment upon reducing the applied field to zero. This trapped flux often referred to as the remanent moment M_R is analogous with remanent magnetization seen in spin glass materials, and in this case it is called isothermal remanent magnetization (IRM).

When cooling the superconductor material from above T_c in the presence of a magnetic field (FC), magnetic flux penetrates the superconductor material at high temperature, and gets trapped upon further cooling. A positive magnetic moment can be measured below Tc, when the applied field is reduced to zero. This remanent "trapped" moment is known as thermal remanent magnetization (TRM) again in analogy with spin-glass material. In another words, a remaining moment in the sample can be obtained by turning off the field after magnetizing the sample by either ZFC or FC methods [12].

3.2 Remanent Magnetization

The magnetization of non-ideal superconductor is non-reversible for applied fields that exceeds the lower critical field H_{c1}. The irreversibility is clearly exhibited in the pressure of remanent magnetization. Non-ideal superconductors are characterized by pinning centers that arise from defects, and inhomogeniety in crystalline structure. These centers provide a local environment at which flux lines are pinned in a relatively stable configuration. This trapped flux represents the remanent magnetization in zero applied magnetic field. Remanent magnetization $M_{rem}^{(H)}|_T$ provides a sensitive measure of the onset of flux penetration at a given temperature and a changing field mode, see ref.[28].

Experimentally, the remanent magnetization can be obtained from the hysteresis loops by cycling the applied magnetic field (at a fixed temperature) from zero to a certain maximum and back to zero, producing half a hysteresis loop. From this loop, we can obtain the remanent moment M_r which is the magnetization at zero magnetic. The

importance of M_r is that it is a measure of the density of trapped flux inside the sample, which is roughly proportional to the density of pinning centers.

3.2.1 ZFC and FC States

The locus of IRM points and the maximum applied field H_{ap}^{max}, produced after field sweeping is shown in figure 3.1. Measurements were performed in the field range (1 to 90 kOe) and in the temperature range (2 to 80K). Initially, IRM increases rapidly, then approaches saturation near 15 kOe. Above 20 kOe, the IRM essentially saturates at about 10.4 emu/cm^3 . Similar behavior is followed for the TRM state with a saturation value of the remanent magnetization at about 10.6 emu/cm^3. The remanent magnetization M_r (IRM and TRM) is found to decrease with increasing temperature. The general behavior seen in figure 3.1 at 4.2K has also been seen at higher temperature, however, with a smaller initial slope (dM_r/dH) and lower saturation value M_s.

Trofimov et al. found for YBa2Cu3O7-δ that Mrem1/k vs. H/H*(T) follows a universal behavior, with k as a constant of about 2, and H* is the penetration field [27]. Figure 3.2 shows the behavior of the remanent magnetization for the ZFC and the FC states for the full range of temperatures. In Figures 3.3.a and 3.3.b, we present on a semi-log plot the variation of the remanent magnetization with temperature for IRM and TRM respectively. In both cases, the remanent decreases logarithmically with temperature. The saturated IRM decreases with temperature at a faster rate (~ e -0.051T) than the saturated TRM (~ e $^{-0.043T}$). For comparison we present in the same figures the variation of a non-saturated remanent state obtained by applying 5 kOe for the ZFC and the FC state.

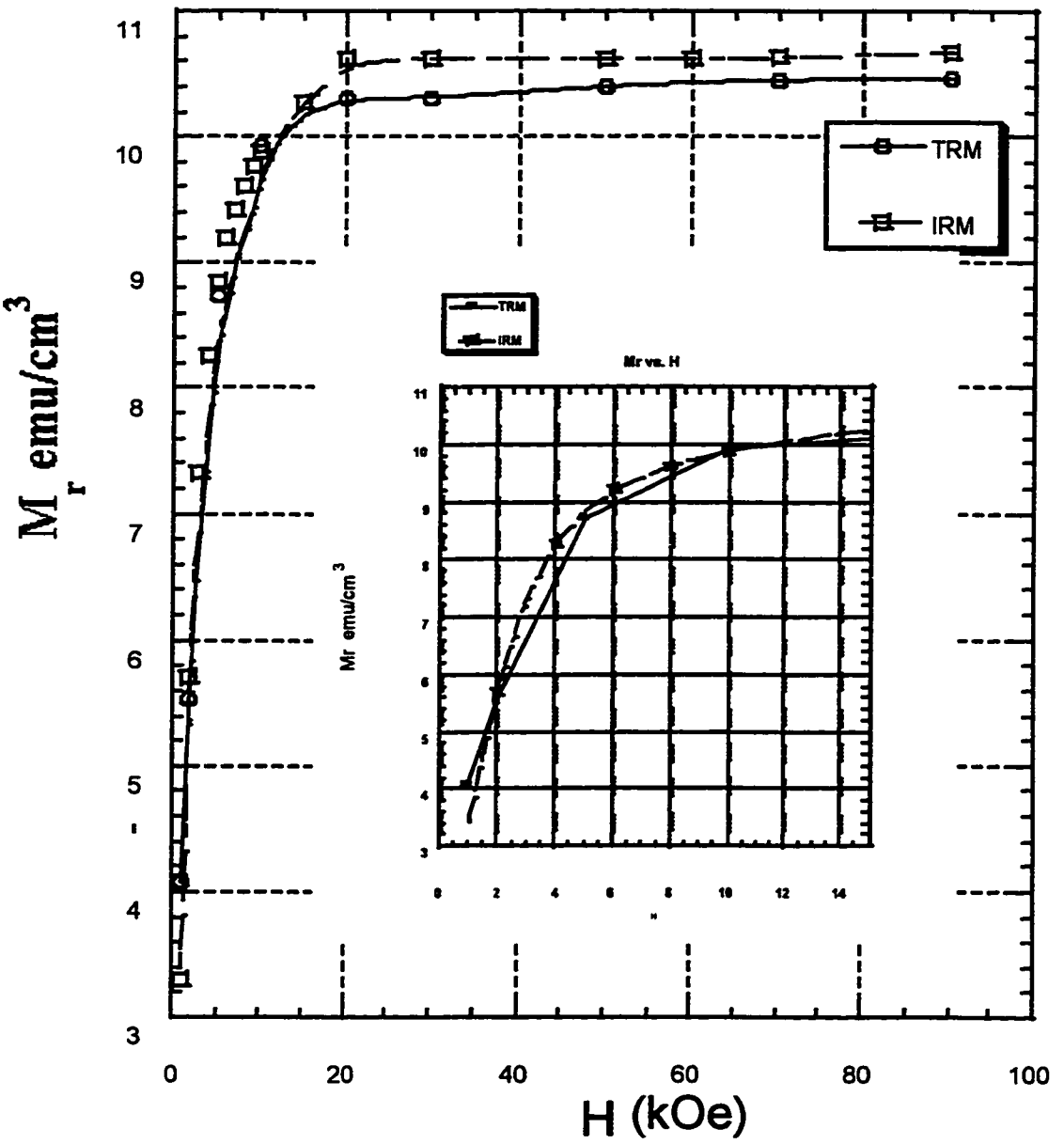

Figure 3.1: M_r vs. H for two regions in this figure, non-saturated (for H=0 to 15 kOe) and saturated (for H=20 to 90 kOe).

In both states, the non-saturated remanent magnetization decreases with slower rate than the corresponding saturated state. The slope of non-saturated IRM is about 0.4 of the saturated slope of IRM. However, the non-saturated TRM slope is about 0.85 of the saturated TRM.

The saturated remanent state has a higher density of trapped vortices than the non-saturated state. Consequently, vortices are closer to each other, and the exchange interaction is stronger (in the saturated state). Since the vortex-vortex interaction is repulsive, this is reflected as a faster decay with temperature in the density of trapped flux. The initial slopes and related parameters ($M_r = \mu_0 \ e^{\gamma T}$) are given in table 3.1, where γ is the slope and μ is a constant.

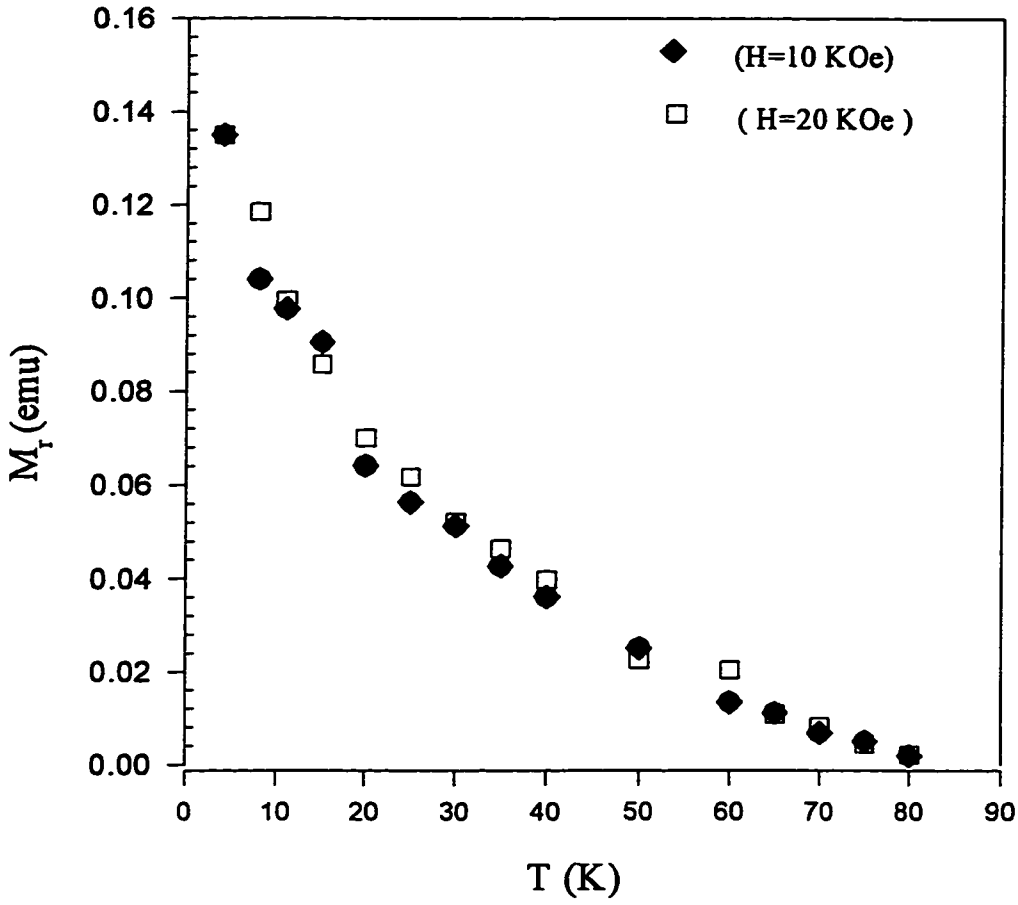

Figure 3.2: Behavior of the M_r for ZFC and FC state for the full range of temperature measurements.

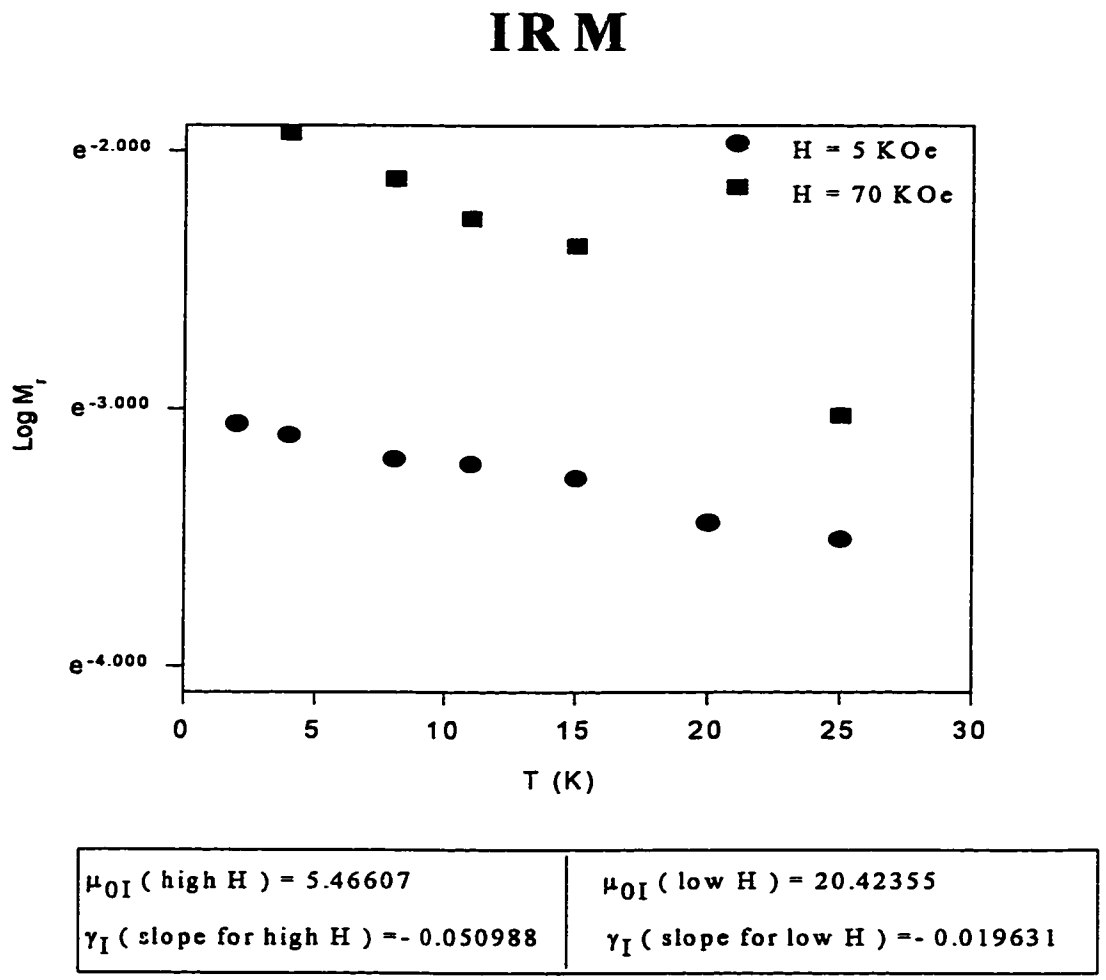

Figure 3.3a: The behavior of M_r for ZFC at different temperatures for high field (70 kOe) and low field (5 kOe)

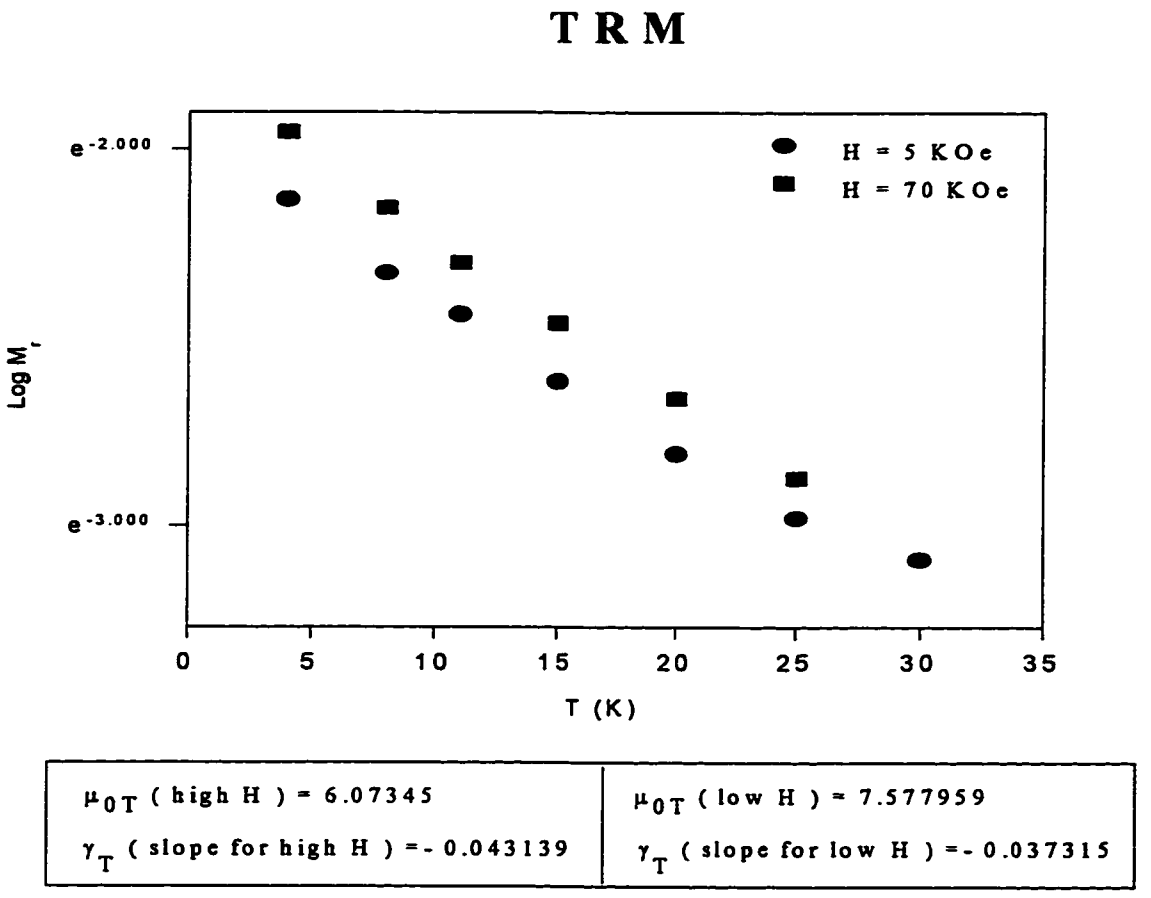

Figure 3.3b: The behavior of M_r for FC at different temperatures for high field (70 kOe) and low field (5 kOe)

Table 3.1

Slopes for the saturated and nonsaturated M_r of IRM and TRM.

State	IRM		TRM	
	Slope γ_T emu/(cm^3.K)	μ_0 const. (emu/cm^3)	Slope γ_T emu/cm^3.K	μ_0 const. (emu/cm^3)
Non saturated	-0.0196	20.42	-0.04	7.58
Saturated	- 0.051	5.47	-0.043	6.07

3.2.2 Scaling Behavior of Remanent Magnetization M_r

Two scaling parameters were used to scale M_r, M* (remanent magnetization at saturation) and H* (field at saturation). An example of the way of finding M* and H* is shown in figure 3.4.

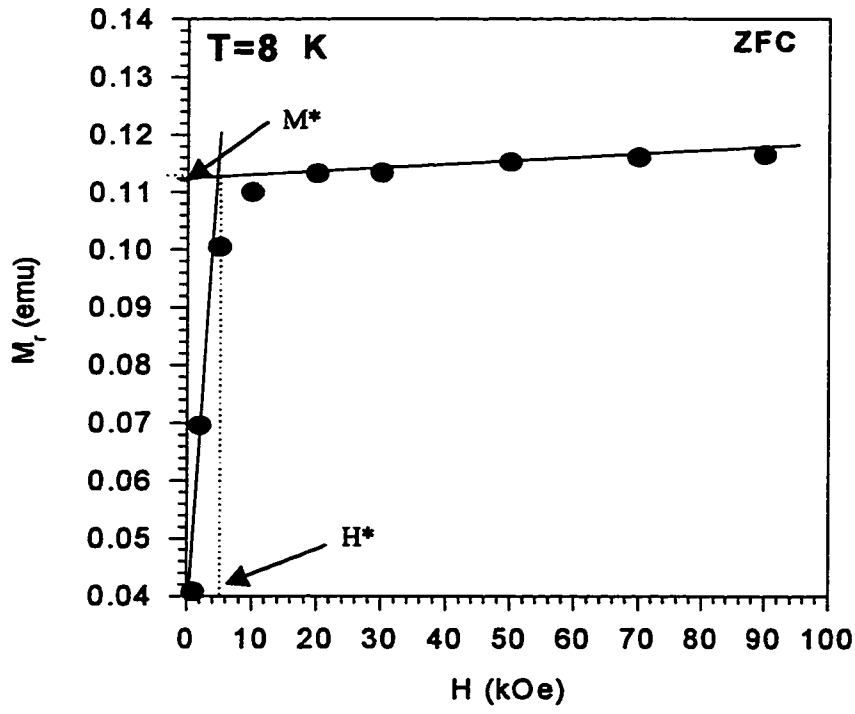

Figure 3.4: The way of finding scaling parameters M* and H* at T=8K for ZFC state.

M* was used to scale M_r axis and H* to scale H axis in figure 3.1 for different temperatures. Figure 3.5 shows the scaling behavior of normalized M_r (M_r/M^*) versus normalized field (H/H*) for the ZFC state. The scaling was achieved for a wide range of temperatures (almost following one single curve) for the initial and saturated part.

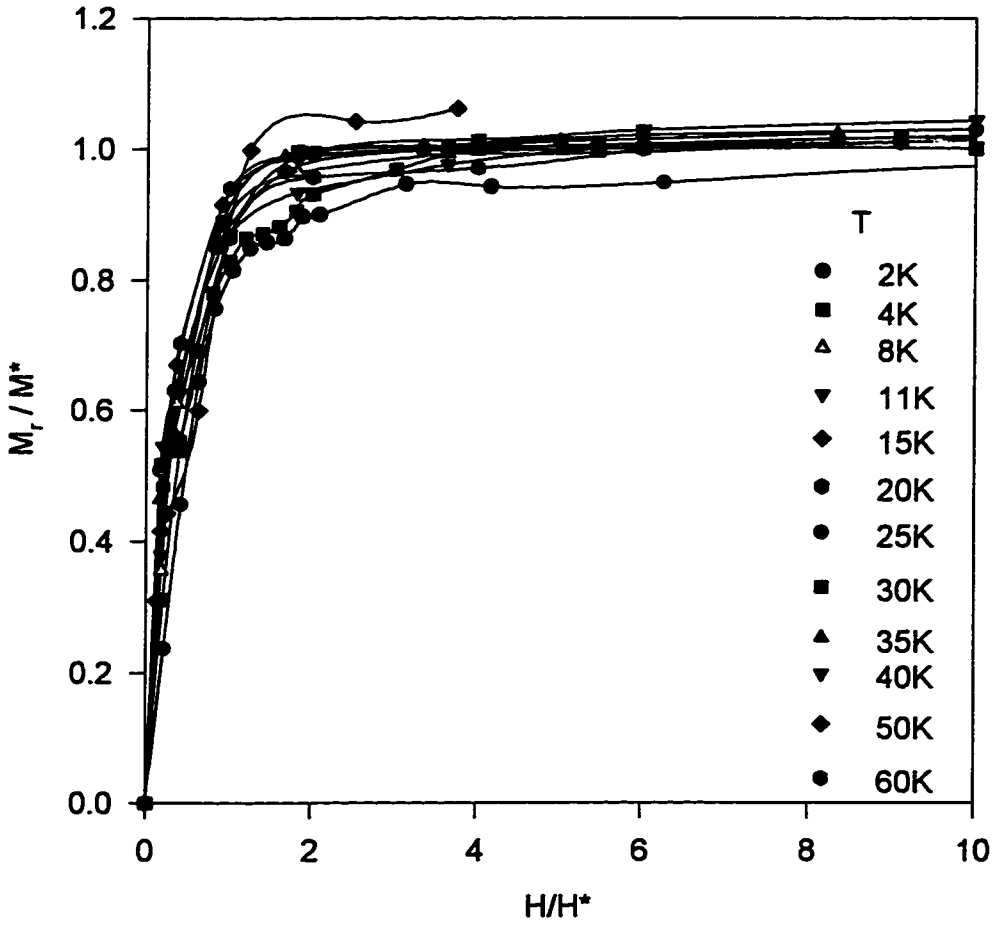

Figure 3.5: Scaling behavior of M_r for ZFC state at a wide range of temperatures (T = 2 to 60K).

3.3 Hysteresis Loops

In the absence of pinning centers, type-II superconductors are ideal and their magnetization is reversible. Moreover, in the presence of pinning centers, type-II superconductors are non-ideal, and their magnetization is irreversible for fields up to an irreversible field, above which the magnetization becomes reversible. In any case, the reversible part of the magnetization near the upper critical field H_{c2} is generally described by the Abrikosov theory, and the irreversible magnetization is commonly described by Bean's critical state model [5,27]. Bean's model describes the field and temperature dependence of the magnetization in the irreversible regime by relating the width of the hysteresis loop at a given field to the critical current [28].

Hysteresis loops are generated by measuring the magnetization of a SC sample while increasing the field from zero up to a maximum value back to zero, then the field is decreased in the opposite direction to the same maximum value, then back to zero to complete a loop. From this hysteresis loop many SC properties can be obtained, such as critical fields H_{c1} and H_{c2}, energy loss and remanent magnetic moment [29].

One of the most extensive hysteresis loops measurements in high temperature ceramic superconductors has been performed by Oussena & Senoussi *et al.* [12]. The negative magnetization first increases almost linearly with applied field with a slope indicating a high degree of flux exclusion (about $-1/4\pi$). Near a lower critical field H_{c1}, the magnetization begins to deviate away from linearity leveling off to a maximum (in the magnitude of the magnetization). Above H_{c1}, applied magnetic field starts penetrating the

superconducting sample, gradually reducing the magnetization of the sample, approaching zero near the upper critical field H_{c2}. When the field is reduced from a high value (typically several Tesla), the magnetization changes sign and usually attains a new plateau that rises to a maximum near zero field.

As the temperature increases, the amplitude of the M-H loop shrinks rapidly and at T* (irreversible temperature where the sample becomes non-hysteretic), the hysteresis entirely disappears at high fields leaving an almost equilibrium (reversible) M-H loop.

From these hysteresis loops, we can obtain:

- The area of hysteresis loop which represents the energy losses in the sample.
- The remanent magnetization M_r, which gives an idea about trapped flux, where M_r is the value of magnetization at a field equal to zero ($H = 0$).
- The critical current J_c, which is the width of hysteresis loop, $J_c \propto \Delta M$.
- The irreversibility field at which the width of the hysteresis loop goes to zero; $\Delta M \sim 0$.
- The pinning forces F_p which are equal to $J_c * H$.

3.4 Scaling Behavior of the Hysteresis Loops:

Hysteresis loops at different temperatures have similar shape and behavior suggesting that they can be scaled to a single curve by using a suitable scaling field H* and magnetic moment [27,29]. Scaling parameters used in hysteresis loops scaling can be used to scale all superconducting properties that can be deduced from hysteresis loops such as critical current, pinning force and remanent magnetization. Examples of hysteresis loops at different temperatures are shown in figure 3.6. The $YBa_2Cu_4O_8$ sample was cooled in zero field from above T_c(~ 80K) to different T(K) and the field was cycled between ± 9 Tesla. The loops are symmetric about the origin.

Several scientists have studied the scaling behavior of the magnetization in different samples. Wolfus *et al.* have used H* (which is the lowest field at which a magnetic flux starts penetrating the sample) to scale the magnetization curves of the $Tl_2Ba_2Ca_2Cu_3Oy$ in the irreversible regime into a single curve. They explained their results in terms of the extended Bean's model, where ($J_c \sim 1/H_n$) and H_{c1} is very small [21]. However, the scaling in this case is satisfied only for a small range of ($H/H_{min} \approx 5$), where H_{min} is the field for which M reaches its minimum [21]. Job *et al.* also used an extended Bean's model to study the scaling behavior in (Bi,Pb)-2223 superconductor using M_{max} and H_{max}, the field at which the virgin magnetization has a maximum magnetization M_{max}. Job *et al.* scaling has been applied over the temperature range (40 to 60K) for $H > H_{c1}$ [31]. Wei *et al.* used two scaling parameters, M_m, the minimum value of the magnetization, and H_m, the field at M_m,

for the first quarter of the full hysteresis loop of the $D_yBa_2Cu_3O_y$ crystal and described the results using an extended Bean's model [32]. Kim *et al.* scaled $Bi_2Sr_2CaCu_2O_x$ films for H> 2 kOe using Bean's model [30].

All of these scaling models used for the hysteresis loops are based on two scaling parameters, and valid only over limited range in temperature and field.

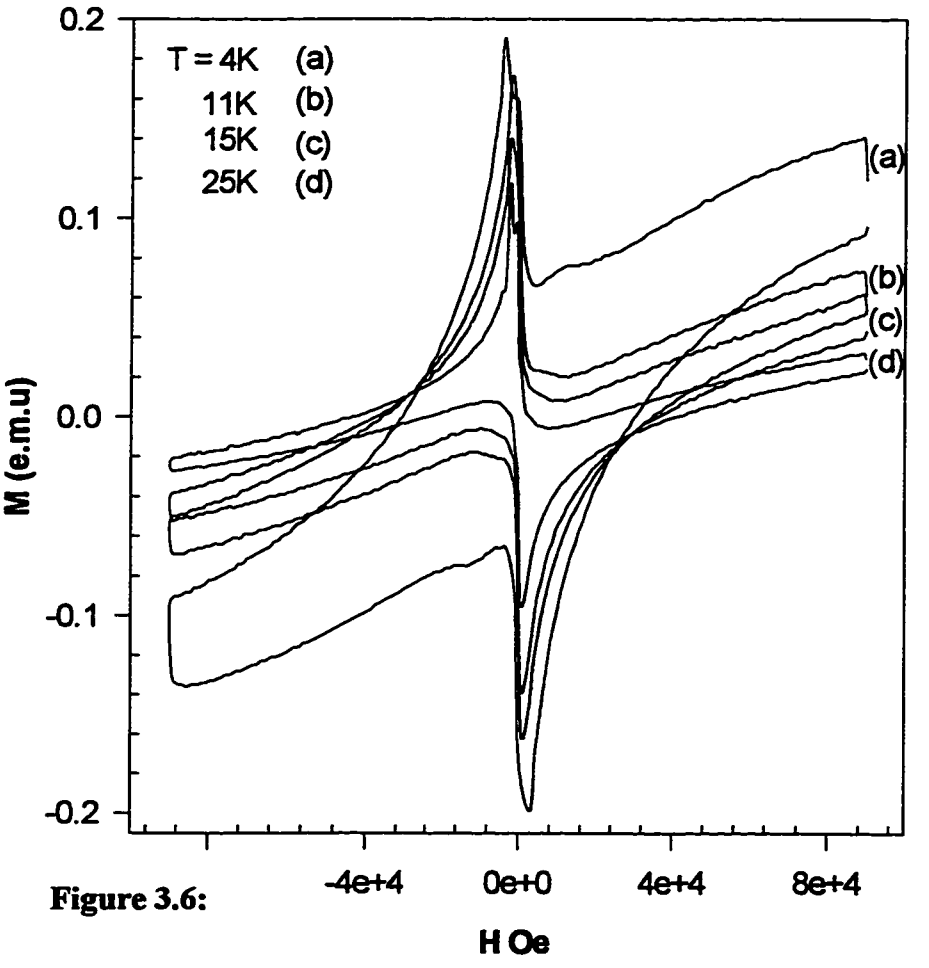

Figure 3.6:

Figure 3.6 : High field hysteresis loops of Y_{124} at different temperatures for the FC state.

One of the difficulties of scaling the behavior of hysteresis loops, is that these loops can be obtained for a variety of trapped flux states. In the following section we illustrate such difficulties, and show that states with different densities of trapped flux may not follow similar scaling behavior at a given temperature. We also show that scaling is followed only for states that are saturated (or close to saturated) trapped flux states.

3.5 Results and Discussion

In order to test the idea that hysteresis loops with different remanent states may not follow scaling behavior, hysteresis loops were measured with a variety of trapped flux states. Upon review of the results obtained in Fig. 3.1, it seemed appropriate to divide the field into two regions: low field region (0 to 15 kOe) with initial linear slope and high field region (20 to 90)kOe. These regions represent non-saturated and saturated trapped flux states respectively. Figure(3.7.a) represents the scaled magnetization M/M_r versus H/H_{max} for non-saturated M_r in ZFC state at 4.2K. Half of the hysteresis is shown, for cycling fields (1, 5, 10, 15 kOe). The data points in the resultant curves do not follow a universal scaling behavior for low cycling field at low temperature. By comparison, we present on the other hand, a different saturated state of the M_r for maximum cycled fields (20, 60, 70, 90 kOe) at 4.2K in Figure (3.7.b). The figure revealed that hysteresis loops closely follow scaling behavior for the data points obtained by cycling at higher fields (60,70,90 kOe), that resulted in full saturated state.

Measurements performed at higher temperature (T=25K) and repeating the plots for the non-saturated and saturated regions are shown in figure (3.8a). For the non-

saturated region (H= 2, 5, 10 kOe) the data points still do not scale very well. However, the curves are closer to each other than what we have seen at 4.2K, (Fig. 3.7.a). While for the saturated region (H=20, 60, 70, 90 kOe) , the scaling behavior is becoming more clearly defined especially for the highest applied fields, this result is shown in Figure 3.8 b (H=20, 50, 70, 90 kOe). See also figure 3.9 (H=10, 20, 30, 50 kOe) for T=35K.

As the temperature increases, the saturated remanent magnetic states are pushed down in field, i.e., the saturated state is being achieved at lower field. Moreover, the reduced hysteresis loops (M/M_r vs. H/H_{max}) closely approach universal scaling behavior upon increasing the temperature. Measurements performed for the FC states are shown in figures (3.10) ,(3.11) and (3.12). These figures show that the observed scaling behavior exists at higher temperature and for higher cycling fields. The figures also reveal that scaling behavior is being obeyed more clearly in the FC states than the corresponding ZFC state.

Chapter 5 introduces a one parameter scaling model to scale pinning force, critical currents and hysteresis loops and also points out a possible source of difficulties that causes the hysteresis loops not to follow a proper scaling behavior.

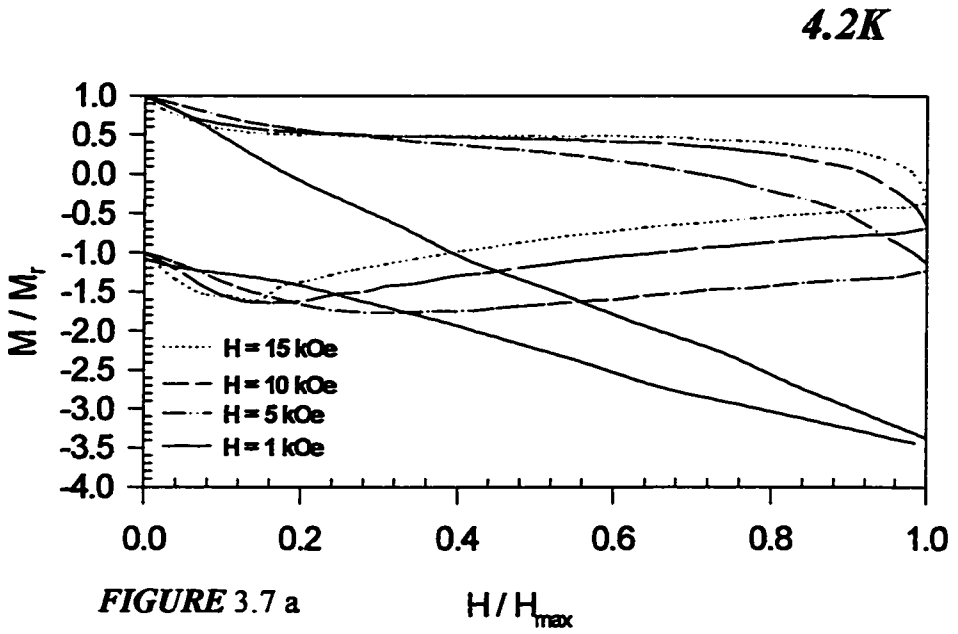

FIGURE 3.7 a

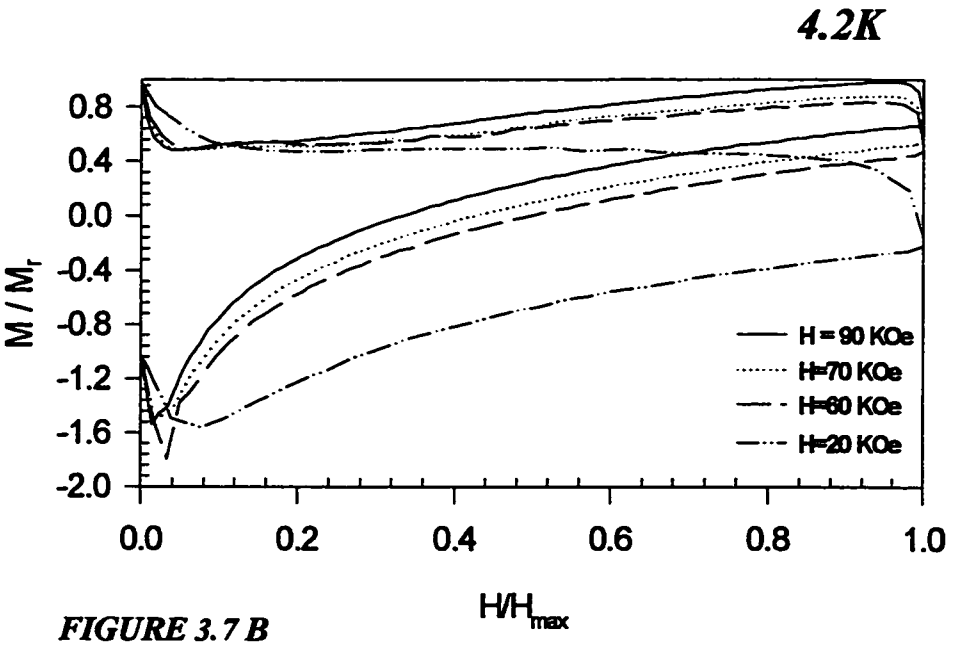

FIGURE 3.7 B

Figure 3.7: M/M_r vs. H/H_{max} for non-saturated M_r (H=1,5,10 and 15 kOe), and saturated M_r (H= 20,60, 70 and 90 kOe).

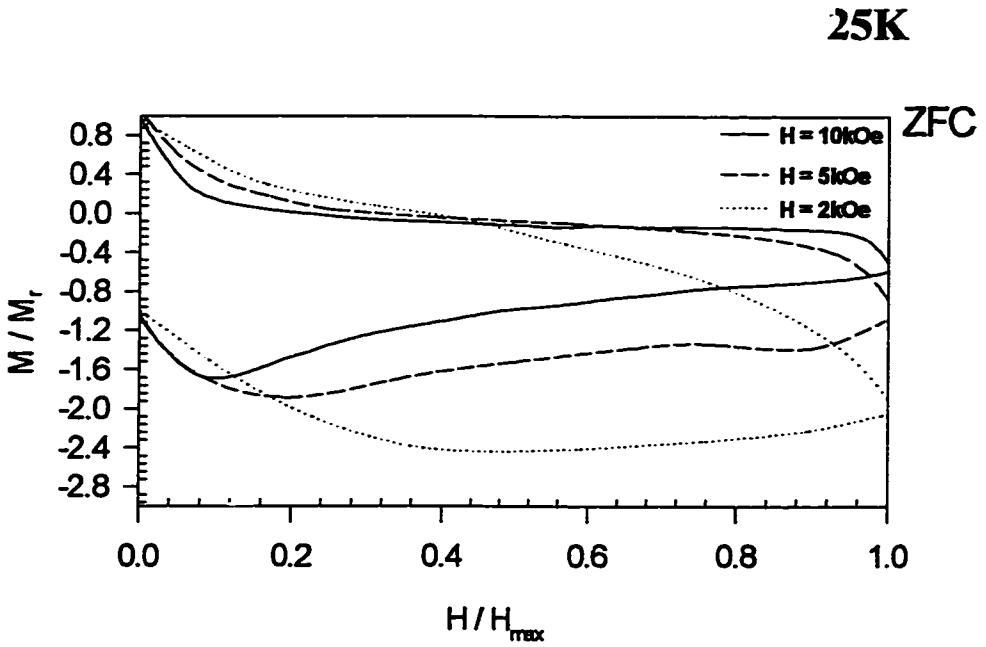

Figure 3.8a

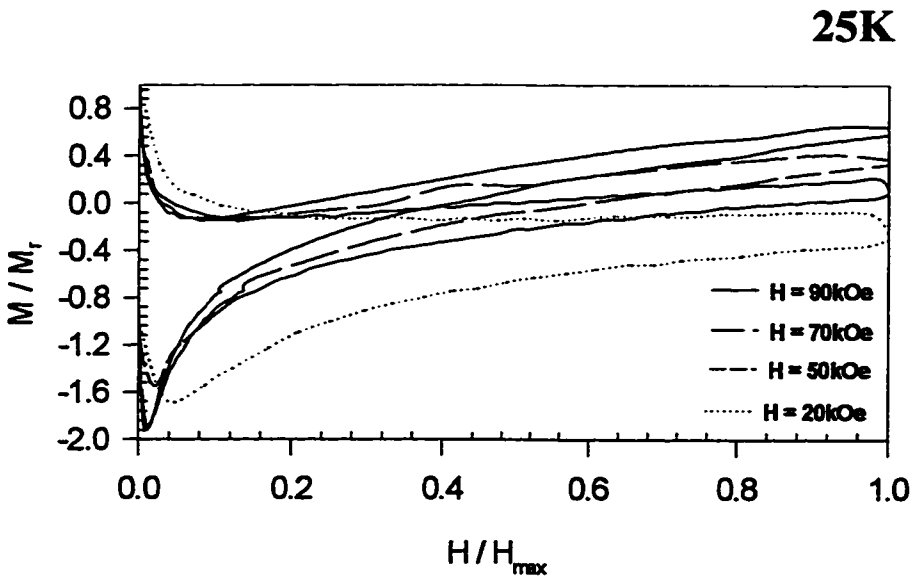

Figure 3.8b

Figure 3.8: M/M_r vs. H/H_{max} for non-saturated M_r (H=2,5 and10 kOe), and saturated M_r (H= 20,50, 70 and 90 kOe).

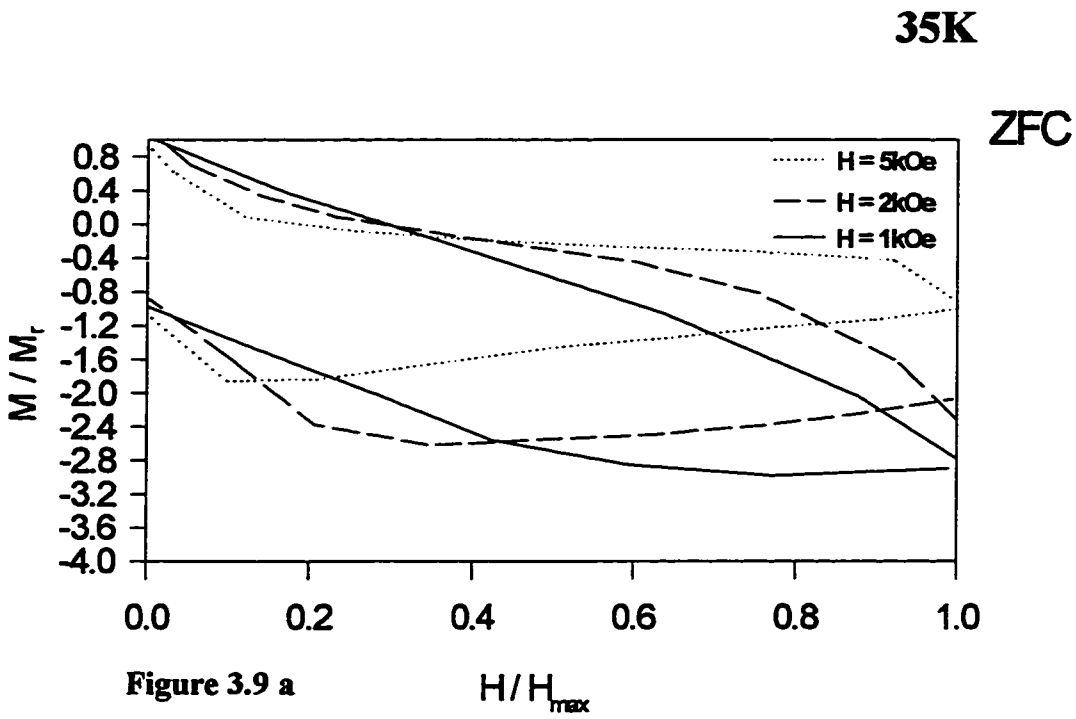

Figure 3.9 a

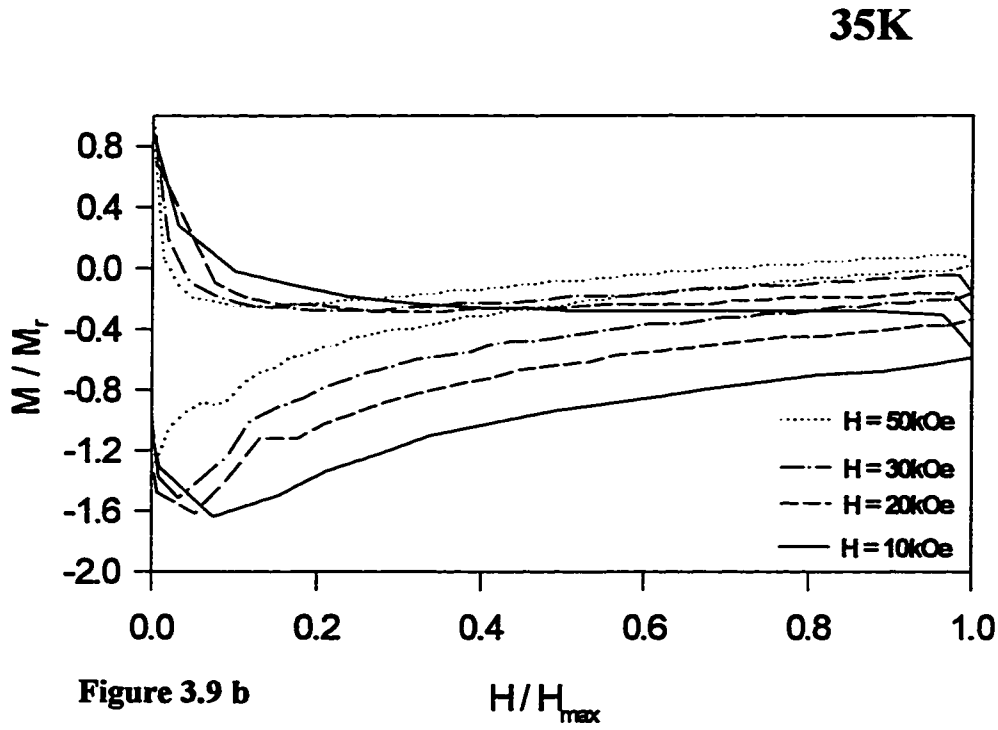

Figure 3.9 b

Figure 3.9 : M/M_r vs. H/H_{max} for non-saturated M_r (H=1,2 and 5 kOe), and saturated M_r (H= 10, 20, 30 and 50 kOe).

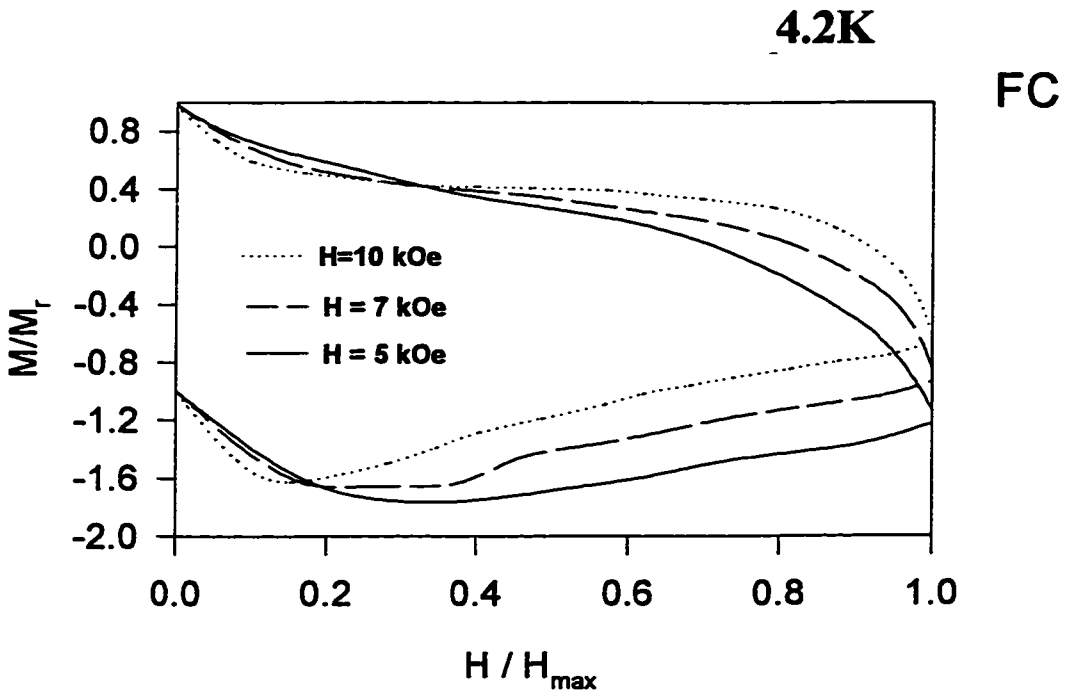

Figure (3.10a)

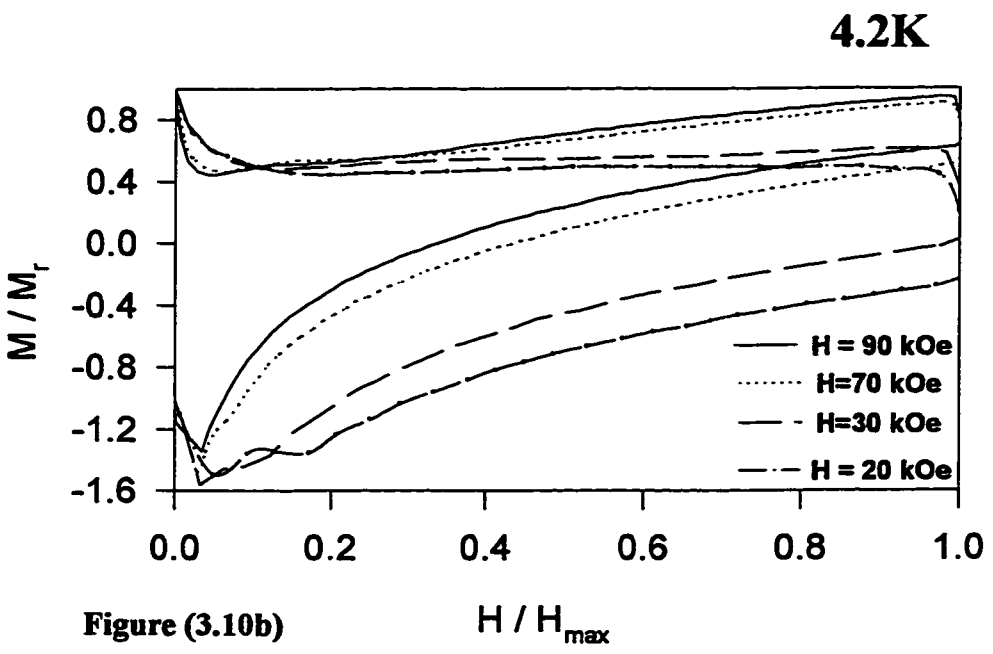

Figure (3.10b)

Figure 3.10: M/M_r vs. H/H_{max} for non-saturated M_r (H=5, 7 and10 kOe), and saturated M_r (H= 20,30, 70 and 90 kOe).

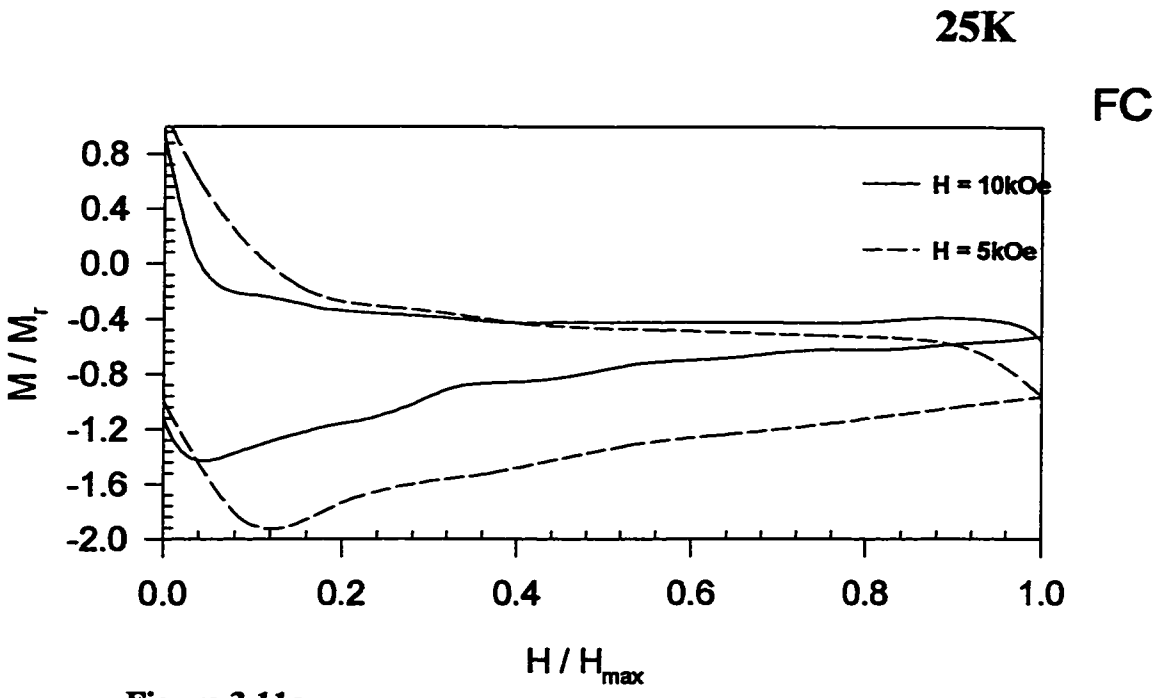

Figure 3.11a

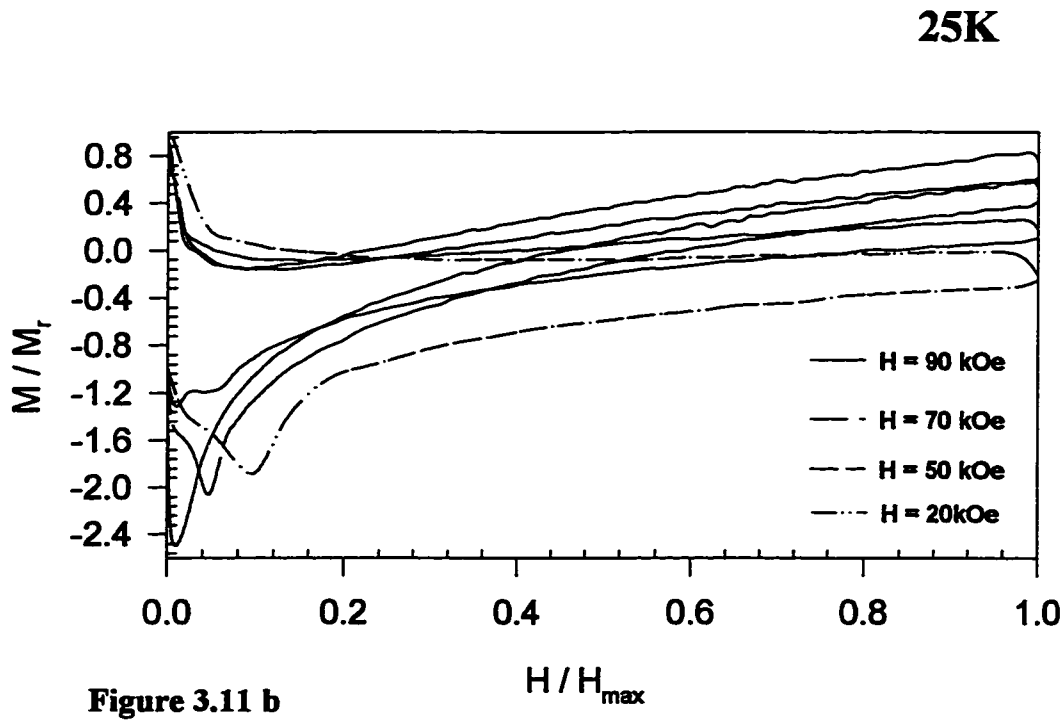

Figure 3.11 b

Figure 3.11: M/M_r vs. H/H_{max} for non-saturated M_r (H=5 and10 kOe), and saturated M_r (H= 20,50, 70 and 90 kOe).

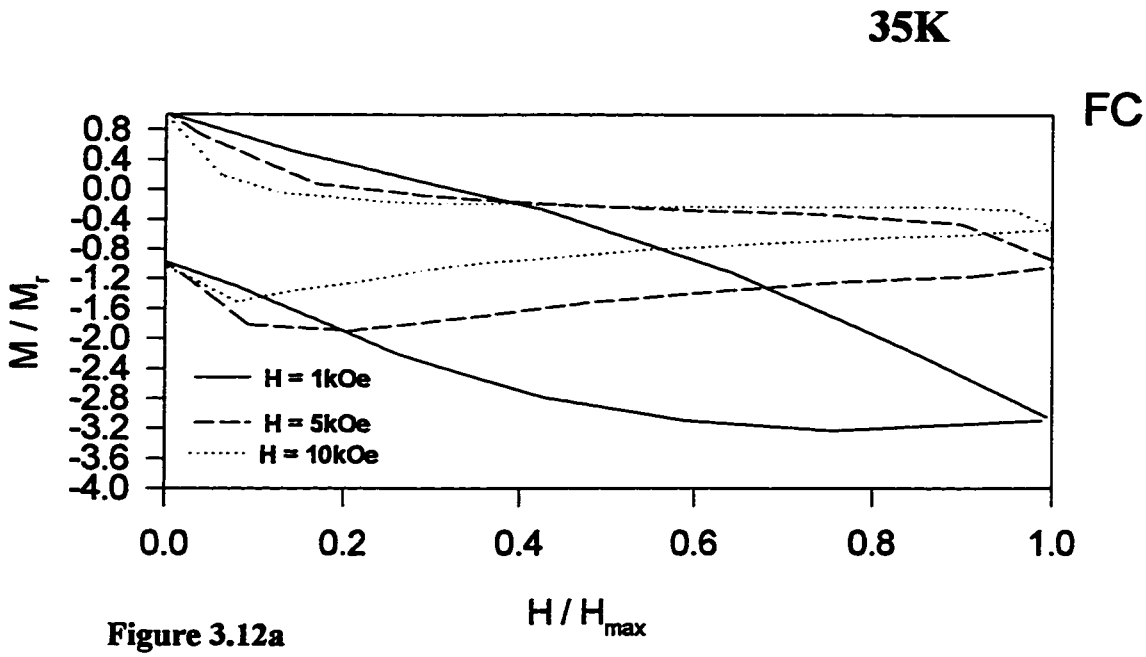

Figure 3.12a

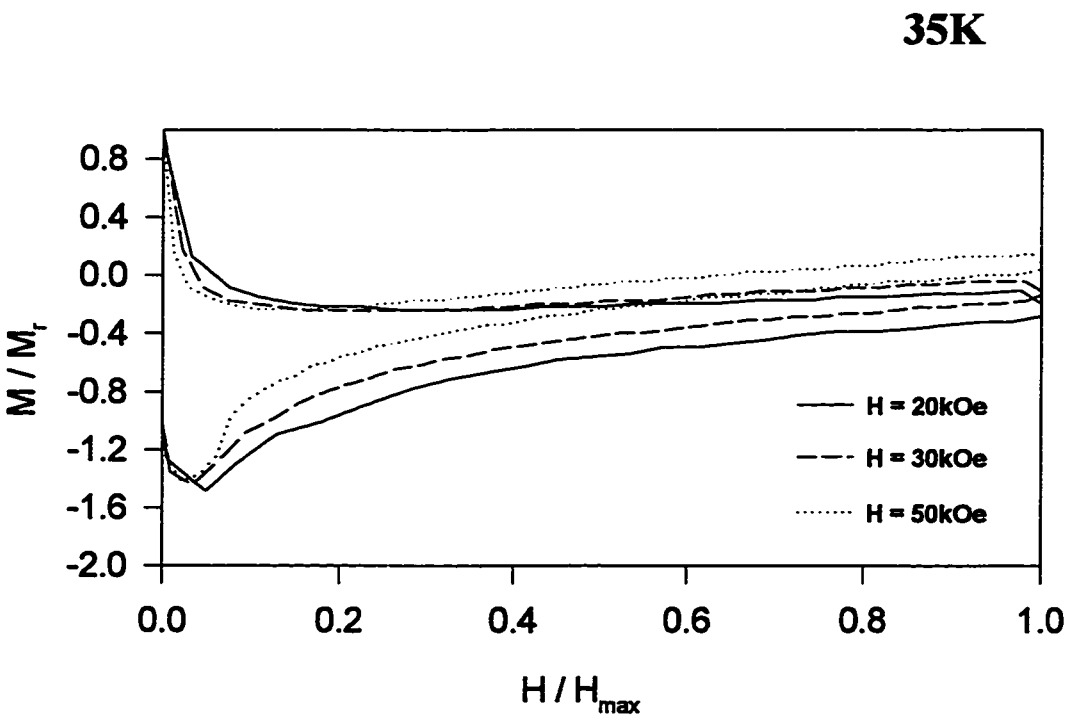

Figure 3.12b

Figure 3.12: M/M_r vs. H/H_{max} for non-saturated M_r (H=1,5 and10 kOe), and saturated M_r (H= 20,30 and 50 kOe).

3.5 Conclusion:

Motivated by the idea that hysteresis loops obtained for different trapped flux states may not follow a single scaled loop; we found that, the IRM and TRM non-saturated states do not follow universal scaling behavior. Using a two scaling parameter scaling method, H_{max} and M_r, it was found that the best scaling behavior is satisfied by high field and high temperature for the saturated region.

CHAPTER 4

Magnetic Energy Losses

4.1 Introduction

Alternating magnetic fields produces irreversible motion of the vortices in type-II superconductors. Alternating currents (Ac) in the superconducting state also have a similar effect. Work done by the external field in moving these vortices can be expressed as energy loss in the superconducting state [33]. Low energy losses are the main attraction in any practical application of SC. In conventional type-II superconductors, a surface barrier for flux motion can reduce AC losses and the addition of a steady direct current (DC) field leads to a further decrease of the losses [34].

These energy losses can be divided into three types, or three different mechanisms. These are: 1) surface losses, which is caused by the movement of the vortices in and out the sample, 2) annihilation losses, due to moving vortices in the

opposite field direction and, 3) bulk pinning losses, which depends upon the extent to which these vortices are pinned [34-36].

For granular superconductors the magnetization is the sum of intergranular and intragranular magnetization, and the energy loss is the sum of intergranular and intragranular losses [34]. The magnetic energy dissipated W by the superconductor upon cycling the applied field can be obtained geometrically by evaluating the area of the hysteresis loop generated by cycling the field between two maxima $\pm H_m$. The energy per unit volume per field cycle dissipated is then given as :

$$W = \frac{1}{4\pi}\oint H\, dB \qquad [4.1]$$

Where H is the applied DC magnetic field and B is the volume average of the local field, from [29], [37].

Bean's model assumed that the current density is independent of field, i.e. the critical current density is constant, and this leads to a linear dependence of local magnetic field with the distance from the surface of the sample until it reaches the value H_{c1} [34]. For a slab shaped sample, $B=H^2 / 2H^*$, where H^* is the full penetration field and given as:

$$H^* = \frac{\pi D}{5} J_c \qquad [4.2]$$

Where D is the thickness of the slab sample. Integrating eqn. 4.1 using a value for B, one obtains:

$$W = \frac{H^3}{6\pi H^*}, \qquad \text{for } H \le H^* \qquad [4.3]$$

This cubic energy loss dependence on the maximum field is commonly known as Rayleigh cubic dependence.

For high field, the loss approaches saturation linearly with H, i.e. $W \propto H$ [29]. Ziq *et al.* studied the energy losses in a $(Bi,Pb)_2Sr_2Ca_2Cu_3O_{10-\delta}$) and they found that total energy loss, trapped flux and the diamagnetic contributions decrease exponentially with

increasing temperature[38]. Recently Pramana *et al.* have studied the energy loss in polycrystalline $YBa_2Cu_3O_{7-\delta}$ with varying oxygen content and found that the behavior of the energy loss, which depends on the maximum cycling field, is divided in to two regions, an initial linear region and a saturated region and the varying of oxygen content (x) reflects on the slopes of the initial regions [39].

4.2 Energy Losses in ZFC and FC States

4.2.1 Temperature and Field Effects

Hysteresis loops for ZFC and FC states have been measured at different temperatures below T_c. Figure 4.1 shows selected FC (in 9 Tesla) hysteresis loops obtained at different measuring temperatures (T= 4,11 and 20K) for Y_{124} and with the field cycled between ± 9 Tesla. In this figure, the loops are symmetric about the origin and the area of the loops gradually decreases with increasing temperature.

The same set of experiments was repeated for different cooling fields H_{max}, and for different measuring temperatures below the superconducting transition temperature T_c. For each loop the area of the loop represents the energy loss under the corresponding experimental conditions. Figure 4.2 shows two hysteresis loops taken at T= 4.2K and for two sweeping fields ±9 Tesla and ± 6 Tesla for the ZFC state. The figure reveals that the energy loss W (area) increases by increasing the sweeping field. Similar behavior has been seen for FC state, where we have used the field applied during cooling as the cycling field. The variations of the energy loss with the cycling field and at different temperatures are discussed in the following section.

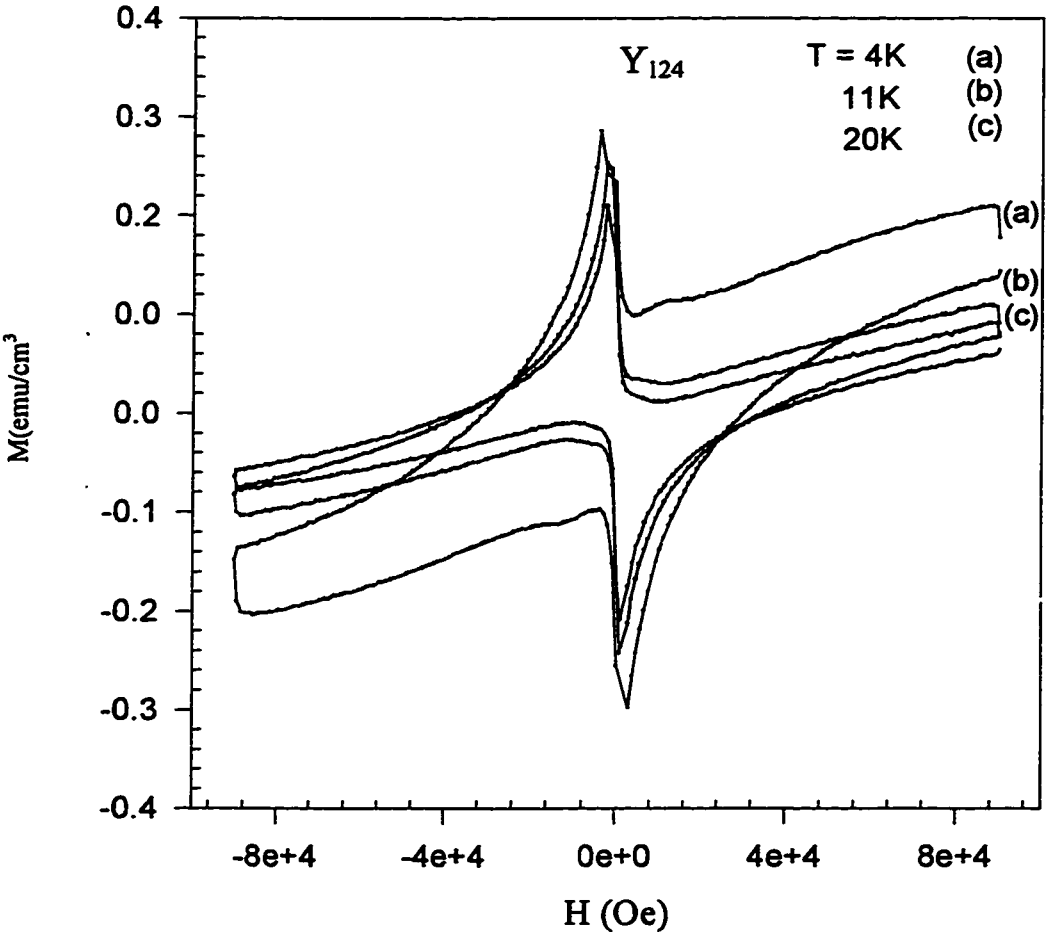

Figure 4.1: Field cooled hysteresis loops produced by cooling Y_{124} in 9-Tesla then cycling it in 9-tesla at different temperatures.

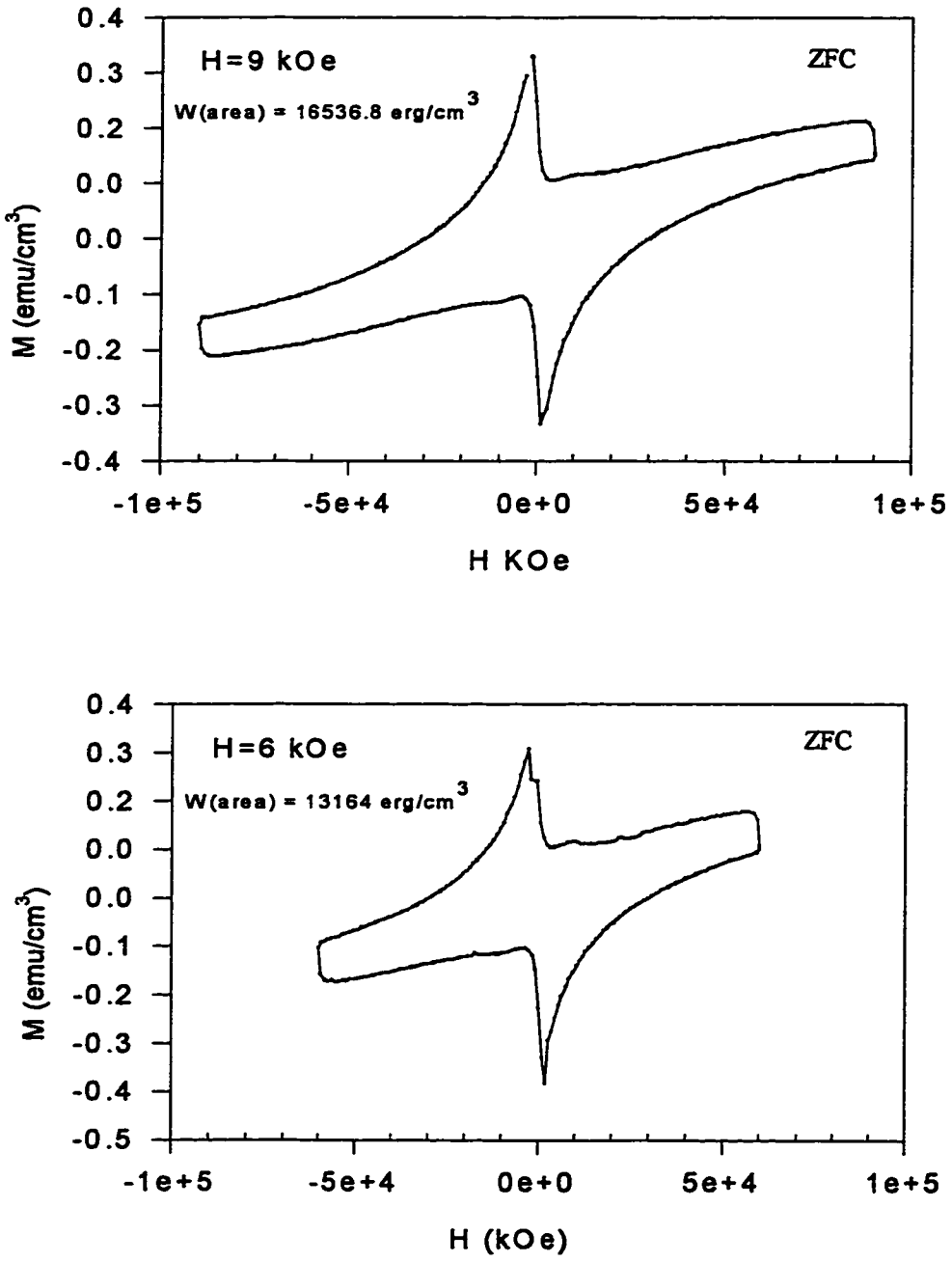

Figure 4.2: Hysteresis loops at 4.2K for different fields.

The areas of the hysteresis loops measured at different temperatures and fields are presented in figure 4.3a as energy losses in ZFC state versus cycling fields for selected temperatures (T= 4,11 and 20K). The replotted data clearly shows that, as the temperature increases the initial slope of each curve is reduced and the saturated values of the energy loss are also reduced. Moreover, the initial slope deviates from H^3-dependence predicted by Bean's model. These remarks are also true for the FC state but with different reducing rate for the initial and saturated part by increasing T, Figure 4.3b.

The similarity of energy losses curves at different temperatures for the ZFC and the FC states, figure 4.3, suggests that they can be scaled by a procedure (sec 4.3) in order to present all these curves at different temperatures in one single universal curve.

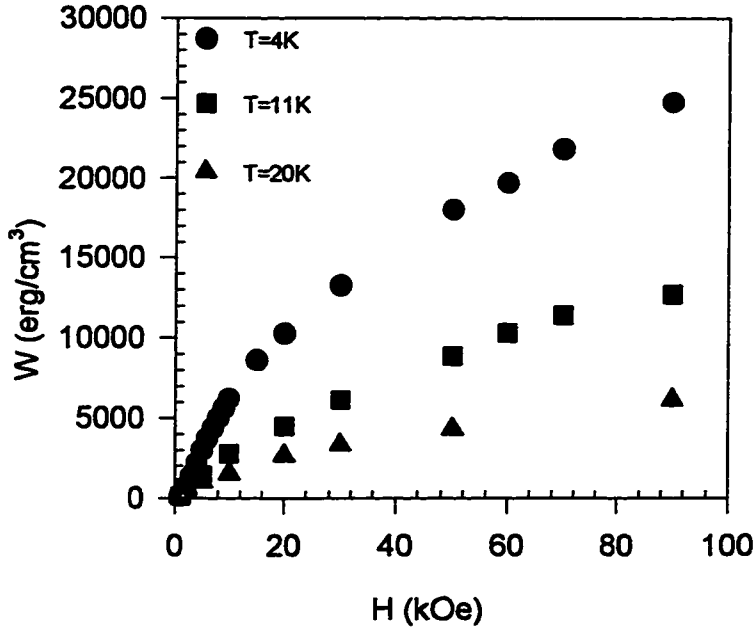

Figure 4.3a : Energy losses W vs. field (H) at different temperatures 4,11 and 20K for ZFC state.

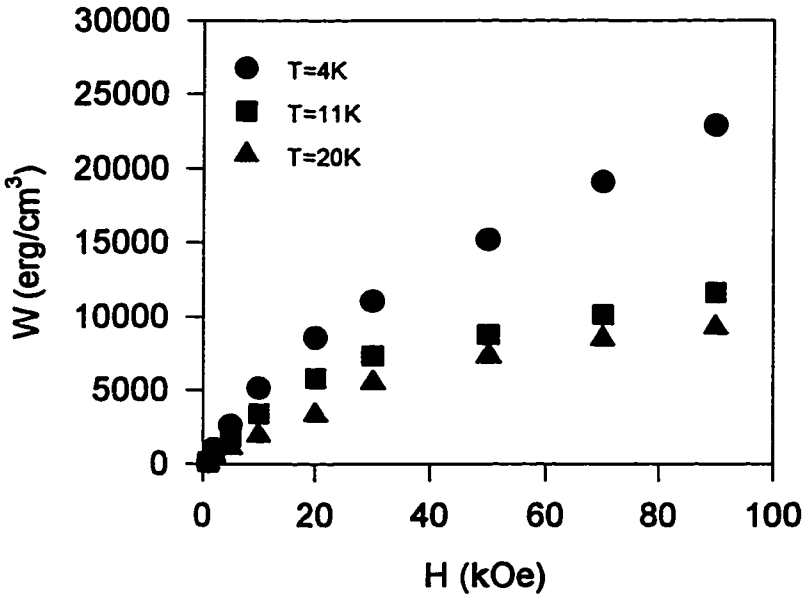

Figure 4.3b : Energy losses W vs. field H at different temperatures 4,11 and 20K for FC state.

4.3 Scaling Procedure:

In order to scale the field H and the energy loss W, the following method was derived. Scaling H is done by dividing all H values by H*, full penetration field at certain temperature T, to obtain the reduced field H/H*. The procedure of finding H* is as follows: from the plot of W vs. H, figure 4.3, we take the intersection point of the initial slope and the final linear (saturation) slope to obtain the corresponding field at that point which is H*. Figure 4.4 gives an example of the procedure of finding H* for ZFC state at temperature 4K. The same procedure is repeated for all temperatures for the ZFC and the FC states. The obtained values are shown in table 4.1. Scaling of the energy loss W is done by dividing W, at certain T, by the maximum energy loss W_{max}, at that temperature, to obtain W/W_{max}. A list of W_{max} for all temperatures is given in table 4.1 for the ZFC and the FC states. Also listed are the values of the energy loss W* at H*. In scaling of the energy loss W* plays the same roll as W_{max}, it has similar temperature dependence. The variations of W_{max} and W* with temperature is shown in figure 4.7.

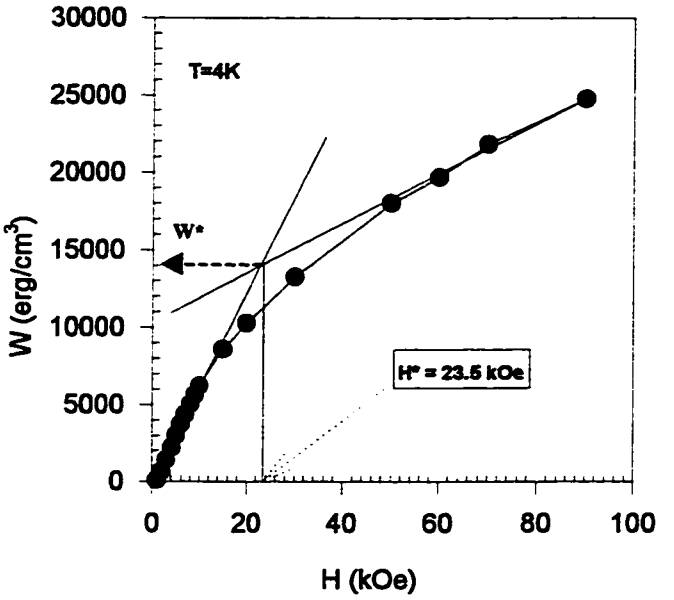

Figure 4. 4: The graphical procedure H* and W* from W vs. H plot (at T=4K) in the ZFC state.

Table 4.1
Data of H*, W* and W_{max} for different temperatures for ZFC and FC.

ZFC				FC			
T (K)	H* (kOe)	W* (erg/cm^3)	W_{max} (erg/cm^3)	T (K)	H* (kOe)	W* (erg/cm^3)	W_{max} (erg/cm^3)
4	23.5	14015.6	24737.180	4	20.0	9573.2	22888.857
8	20.3	9348.8	17173.374	8	17.0	7778.2	14837.922
11	18.7	8825.3	12684.454	11	15.3	6357.2	11623.926
15	15.4	7179.9	8127.923	15	13.6	5160.5	8974.849
20	11.2	2692.5	6150.913	20	11.6	4188.3	6684.767
25	10.0	2587.8	3742.293	25	10.0	2191.4	4212.196
30	8.4	1974.5	3066.407	30	9.0	1869.8	2768.741
35	7.7	1278.9	2004.383	35	7.4	1226.6	2071.694
40	6.3	807.7	1480.850	40	6.5	912.4	1618.464
50	4.8	359.0	1017.150	50	5.7	433.8	753.887
60	4.1	151.1	430.045	60	5.5	237.3	373.952
65	3.9	118.2	194.455	65	5.3	151.1	245.313
70	3.6	70.3	128.640	70	5.2	57.6	93.488
75	3.5	38.1	59.832	75	5.2	38.8	60.730
80	3.4	10.0	29.916	80	5.1	22.6	37.949

4.4 Results and Discussion:

Using the data in table 4.1 to study the behavior of W_{max} with H*, figure 4.5 shows the behavior of W_{max} versus H* for the ZFC and the FC states and it seems that for both curves there are different regions. For the ZFC state there is region (I) from H* = 23.5 kOe to H* = 11.2 kOe, region (II) from H*=10 to 7.7kOe and region (III) from H*=6.3kOe to H*=3.4 kOe. The same is also true for the FC state but with only two regions, region (I) H* from 20 to 6.5 kOe and region (II) H* from 5.7 to 5.1 kOe. In order to have a clearer picture about the behavior of the maximum energy loss with H* and possible scaling behavior, we represent the data in figure 4.6 with log-log scale and compare the slopes of these two regions for the ZFC and the FC states. Figure 4.6 shows that for both states, ZFC and FC, similar behavior is being followed for the initial and final slopes, with a shift in the initial slope. This behavior suggests that we can use the same scaling parameters to scale the energy loss and the field for ZFC and FC states. The slopes of each region, for W_{max}, in figure 4.6 are illustrated in table 4.2.

Figure 4.7 represents the temperature dependence of W_{max} and W* for the ZFC and the FC states on semi-log scale. It appears that for both states the energy loss is decreasing rapidly with increasing the temperature at about the same rate (slope for both states around -0.035).

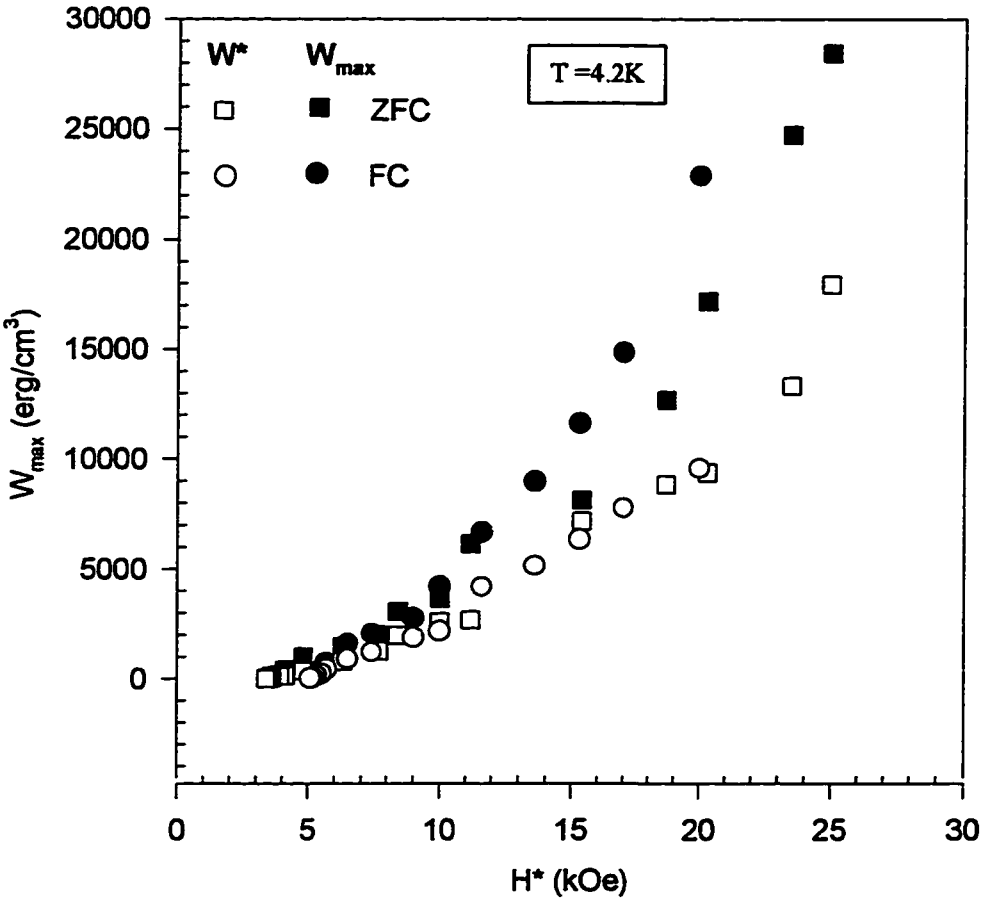

Figure. 4.5 : Behavior of W_{max} and W* versus H* for ZFC and FC states.

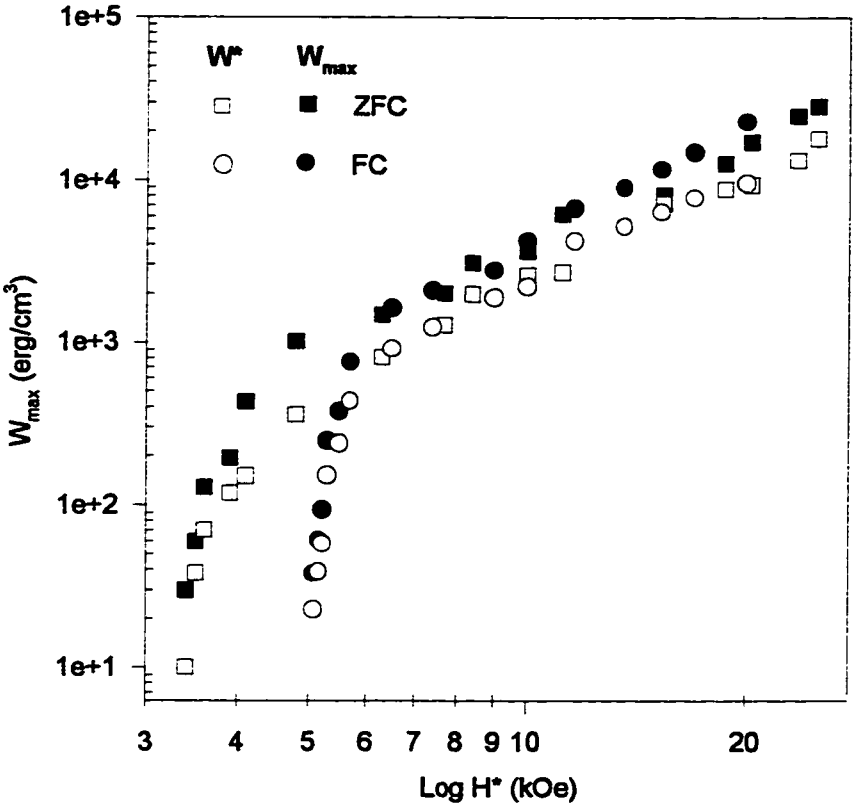

Figure. 4.6 : Log-Log scale of W_{max} and W* versus H* for ZFC and FC states.

Table 4.2

The slopes for the different regions in ZFC and FC states.

Slopes for ZFC			Slopes for FC	
R (I)	R (II)	R (III)	R (I)	R (II)
1.98	2.10	5.15	2.40	25.78

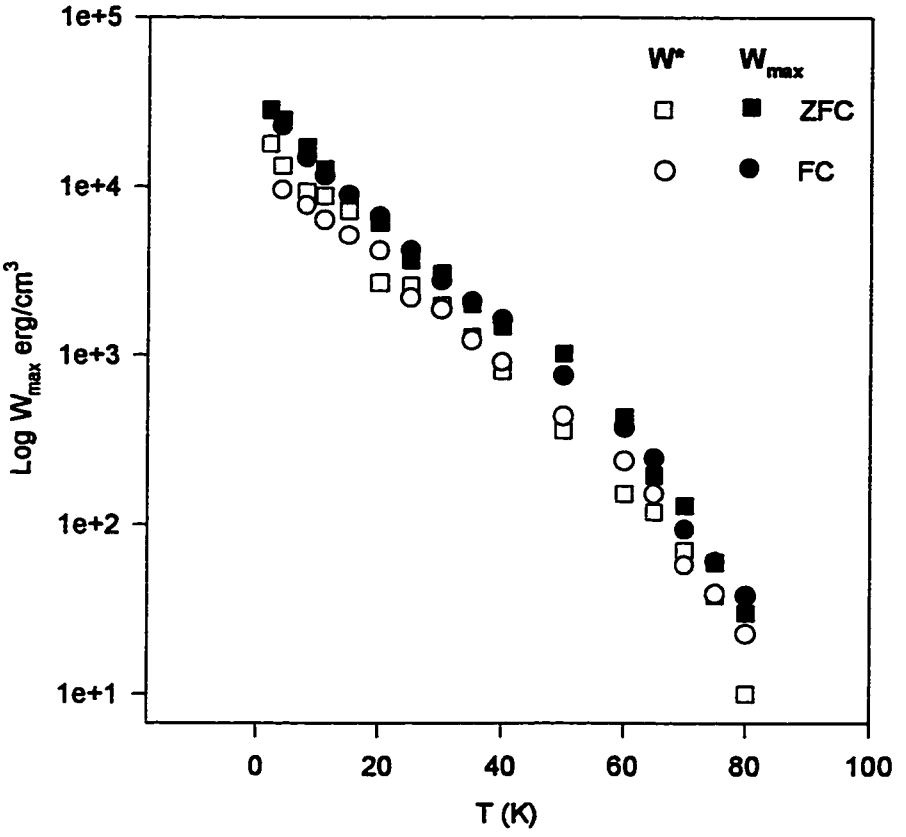

Figure. 4.7 : Temperature dependence of W_{max} and W* for ZFC and FC states.

By scaling the whole region of field and energy losses using scaling parameters mentioned before (W_{max} and H*), a universal plot is created which shows that the scaling behavior of the reduced energy loss W/W_{max} versus the reduced field H/H* for ZFC and FC states. The results are shown in figure 4.8 for temperature measured between 2 and 80K. These results reveal that the data on the initial linear and the saturated parts of the curve follow universable behavior. However, in the intermediate region, the data scatter widely from universal behavior. In order to study the scaling behavior in more detail, the plot is divided into two regions deduced from results shown in figures 4.6 (neglecting the intermediate region in table 4.2 for ZFC). Figure 4.9 shows the two parts of the scaling, for the ZFC, without the intermediate region, part (I) from T=4 to 20K and part (II) from T=40 to 75K. The data points (figure 4.9) are following almost one single curve for both regions. A similar procedure is used on the FC state as shown in figure 4.10.

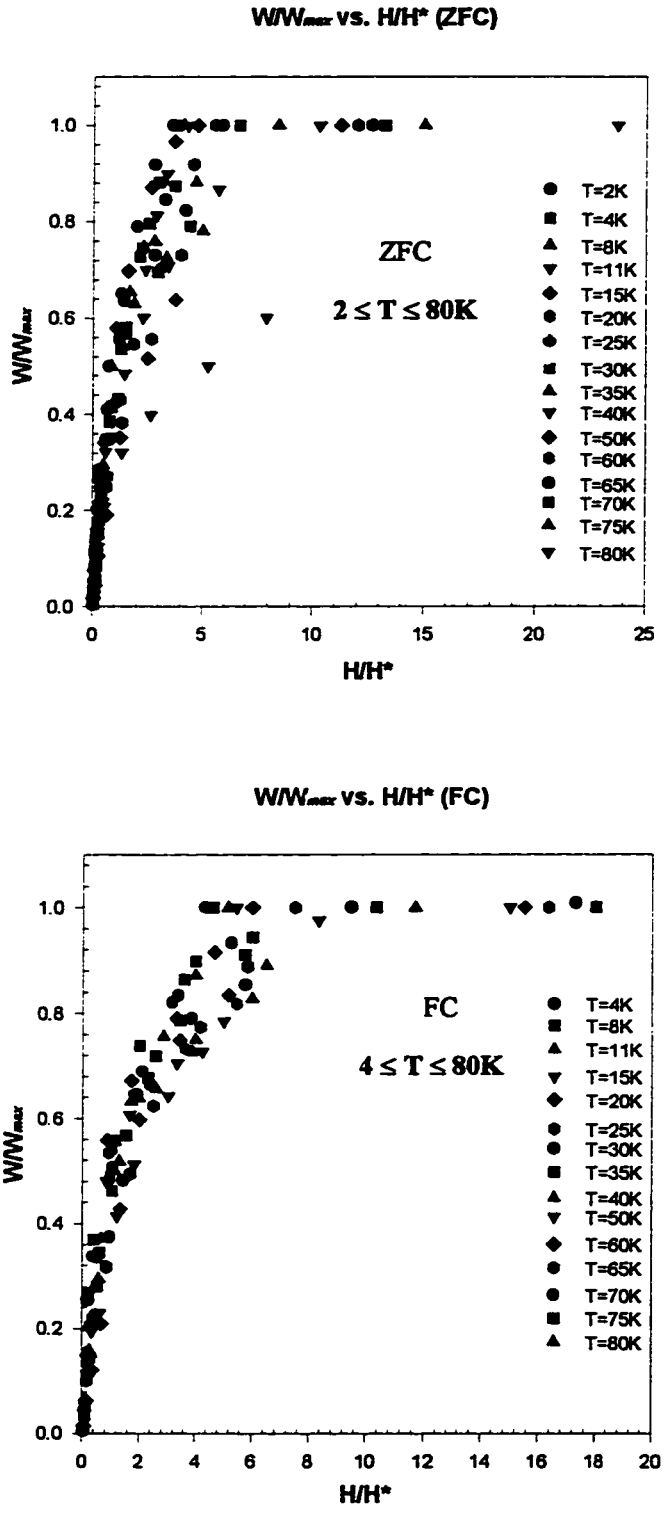

Figure 4.8: Scaling energy losses and field for whole range of data for the ZFC and the FC states.

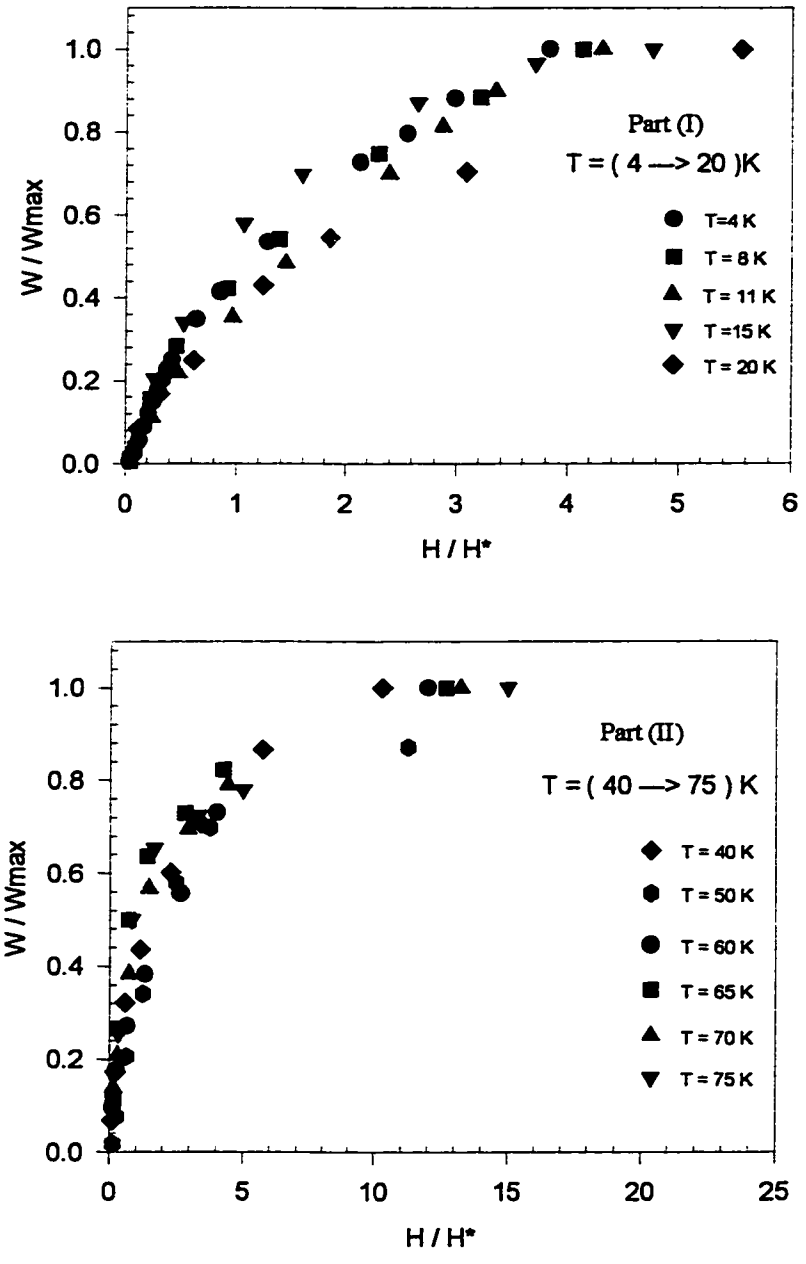

Figure 4.9: The scaling of part (I) and part (II) for the ZFC state.

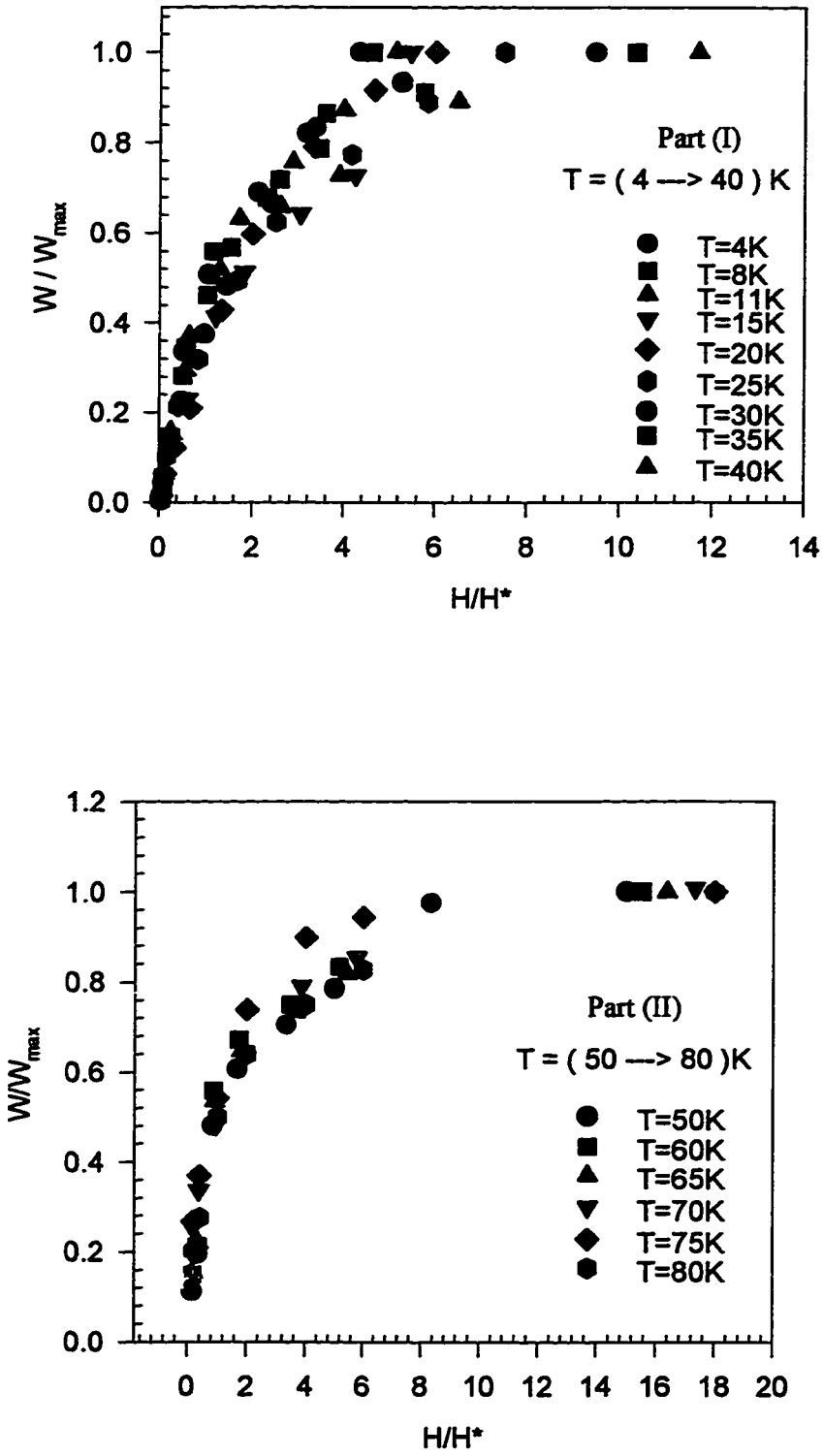

Figure 4.10: The scaling of part (I) and part (II) for the FC state.

4.5 Conclusions:

In this chapter the factors that affect energy losses and its scaling for the superconducting case are studied. These factors are the field and the temperature. It was found that the energy losses decrease for increasing temperature while the energy losses increase for increasing the field, at a given temperature. These losses are due to the motion of vortices inside the SC samples. Also we concluded from figures 4.5 and 4.6 that there are different behaviors, at least two, of energy losses in the SC samples. In the first region, the energy loss is due to the motion of vortices with respect to each other and losses in the second region is due to the motion of vortices as a whole as a rigid bundle inside the sample. This behavior of collective motion of the vortices is reflected as energy losses in the saturated region with linear field dependence. Scaling was performed for the two parts shown in figures 4.9 and 4.10. From these two figures, we observe that the scaling for the FC state is being followed in a more clear manner than for the ZFC state.

CHAPTER 5

Scaling of Critical Current and Pinning Force

5.1 Introduction:

When a magnetic field is applied between Hc_1 and Hc_2 on a type-II superconductor, the magnetic field penetrates the SC sample in selective regions, known as vortices of normal state. In between the vortices, the sample is in the SC state. In this mixed state, the magnetic flux penetrates the material in the form of flux lines, each carrying a single flux quanta Φ_o [5]. Cycling the applied field, generates hysteresis loops that relates the magnetization M and the applied magnetic field H.

Hysteresis behavior is an irreversible behavior of the magnetization caused by internal defects in type-II superconductors. These defects create pinning centers (potential) that interact with flux-lines of the penetrated magnetic field in the mixed state. The flux lines (vortices) are said to be trapped at these centers by pinning forces P_f that

are proportional to the gradient of the pinning potential. The width of the hysteresis loop is a reflection of the strength of the pinning potential. Bean was the first to point out that the width of the hysteresis loop is also proportional to the density of the critical current through his model [29].

The basic idea of Bean's model for a type-II SC is the critical current density. In the superconducting state, there exists a limiting macroscopic SC current density J_c that a hard (type-II) SC can carry. Moreover, the model assumes that this current density is independent of field, i.e.

$$J_c(H) = J_c(0) = \text{constant} \qquad [5.1]$$

where $J_c(0)$ is the critical current density at zero applied field.

The hysteretic magnetization is related to J_c through a modified Ampere's Law:

$$\nabla \times h = \frac{4\pi}{c} J_c \qquad [5.2]$$

where h is the local magnetic induction inside the SC and the critical current density J_c is related to the width of the hysteresis loop through :

$$J_c = 17\ (\Delta M)/R\ ; \qquad [5.3]$$

where ΔM is the width of the hysteresis loop $=(M^- - M^+)$ in emu/cm^3, and R is the average radius of the sample perpendicular to the field [29].

The importance of studying J_c and P_f is that they play a major roll in practical application. It is a continuous quest to increase Jc for producing higher and higher magnetic fields through increasing the density of pinning centers and pinning force P_f by, for example, ion implantation or substitutions and controlled irradiation [29,40,42].

In this chapter we examine the behavior of pinning force P_f and critical current density J_c at different temperatures and fields. We also introduce previous work on scaling properties of P_f and J_c, which is often based on two scaling parameters. We also introduce a new scaling procedure that constitutes the basis for a one parameter scaling model we propose.

The new scaling method is different from the previous work [30] where two fitting parameters have been used in scaling argument and can be applied over a much wider range of temperature. It can also be applied to various magnetic properties like J_c for example. Our method is based on using one scaling parameter to scale both J_c and P_f at the same time.

5.2 Critical Current:

The critical current J_c has been evaluated using equation 5.3. The hysteresis loop is expressed in emu/cm^3, and R is the average radius of the grains $\approx$10 μm. The variation of the critical current with field at different temperatures is shown in figure 5.1 for the ZFC state, where the field was cycled between ± 9 Tesla. Initially, J_c rapidly decreases with increasing H, then gradually decreases with H, almost becoming field independent at high fields. A similar behavior is seen for the FC state. The small fluctuation that is observed at high H represents the noise level in our measurements. Figure 5.2 also presents measurements performed at different temperatures for the FC state. As the temperature is increased, the critical current decreases gradually. The overall shape of

these curves at different temperatures are similar suggesting that they can be scaled using an appropriate procedure, as discussed in section 5.4.

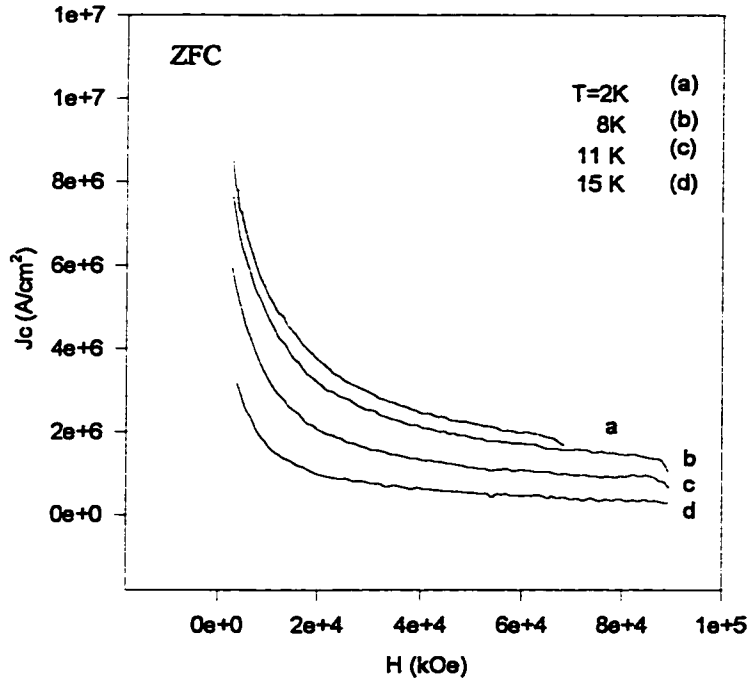

Figure 5.1 : Behavior of J_c with (H) at different temperatures for the ZFC state.

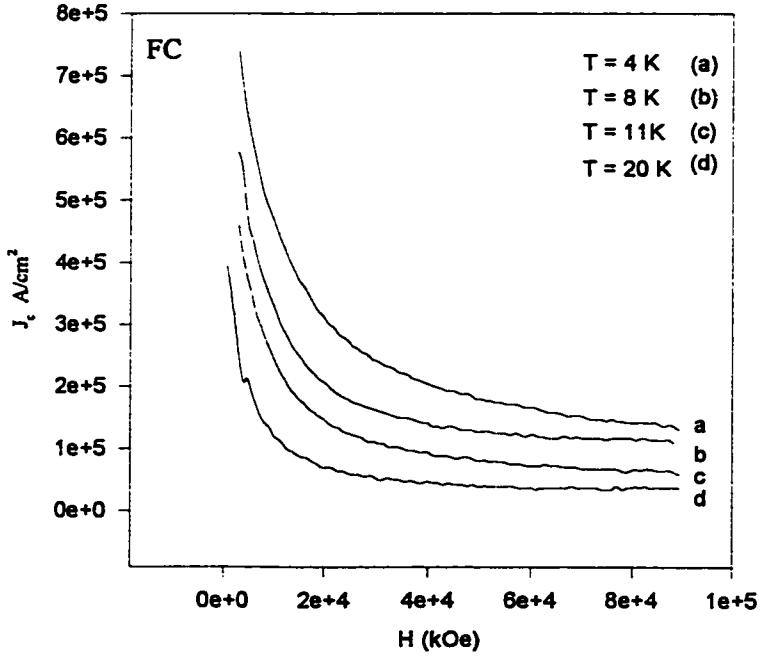

Figure 5.2 : Behavior of J_c with (H) at different temperatures for the FC state.

5.3 Pinning Force:

The pinning force P_f can be readily evaluated from the data presented in figures 5.1 and 5.2, the pinning force is given as $Pf = J_c * H$. The results are presented in figure 5.3 (a) and (b) for the ZFC and the FC states respectively.

At a given temperature, the pining force initially increases linearly, then gradually increases at high field with smaller (saturation) slope than the initial slope. Measurements were performed at different temperatures. The general behavior of the pinning force P_f is that, it decreases with increasing temperature. At high temperature T≥ 15K the pinning force effectively reach saturation. At temperatures close to Tc (~ 75K), not shown in the figure, the width of the loop goes to zero at irreversible field (~ 30kOe), where the pinning force effectively goes to zero.

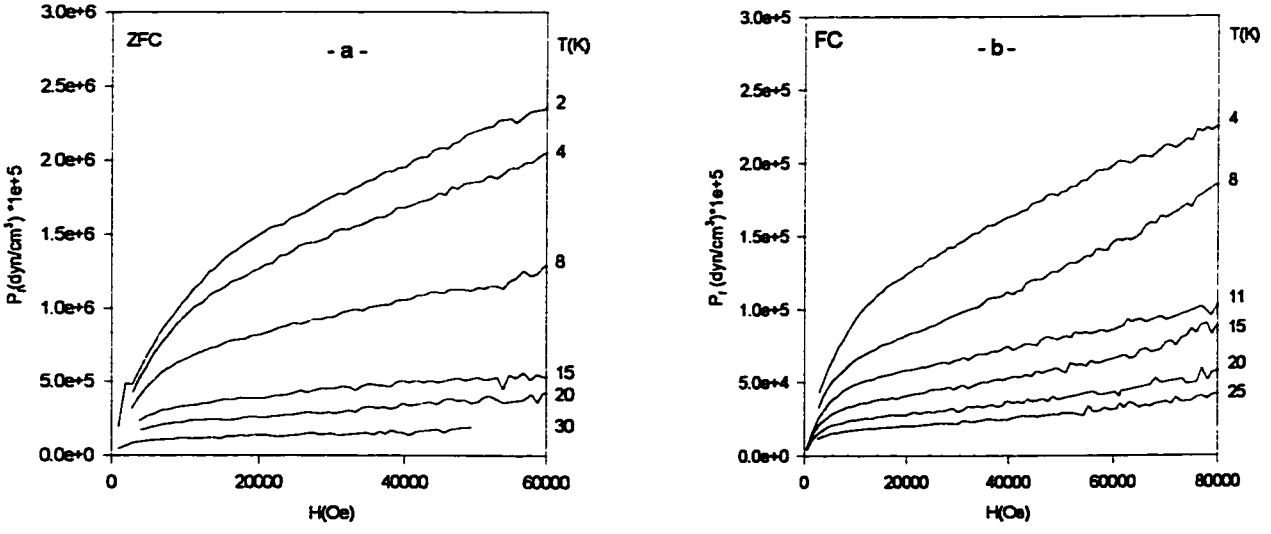

Figure 5.3 : Pinning force P_f versus average field H(av) at different temperatures for ZFC and FC states.

5.4 Scaling Behavior:

There have been many models that describe scaling behavior in pinning force in conventional SC [16] as well as in HTSC [43]. However, very little effort have been done to scale the behavior of critical current. There is no such model in the literature that describes scaling of the current density in a spirit similar to scaling of the pinning force.

Kramer's scaling model [16], among many other scaling models for the pinning force, are mainly phenomenological and based on two scaling parameters. Namely, maximum pinning force P_{max} and one of the following fields H* (field at maximum pinning force), H_{irr} (field at which the width of the hysteresis loop equal to zero), H_{max}, H_{c1} or H_{c2}. Moreover, these models are limited to the case where the pinning force goes to maximum (at H*), then decrease to zero at H_{irr} or H_{max} or at H_{c2} as shown in figure 5.4 [41].

For many high-T_c superconductors, scaling the pinning force is only observed at high temperature close to T_c because H_{irr} or H_{max} can be achieved only at temperatures close to T_c. At high temperatures, fluctuation effects may affect the structure of the flux lines, eventually affecting pinning forces. In other words, there exists a wide range of temperatures where these models are not applicable. In the following section we develop a procedure that overcome such a difficulty. The procedure is based on one scaling parameter that can be used to scale the pinning forces and critical current density at all temperatures. This is discussed in the following section.

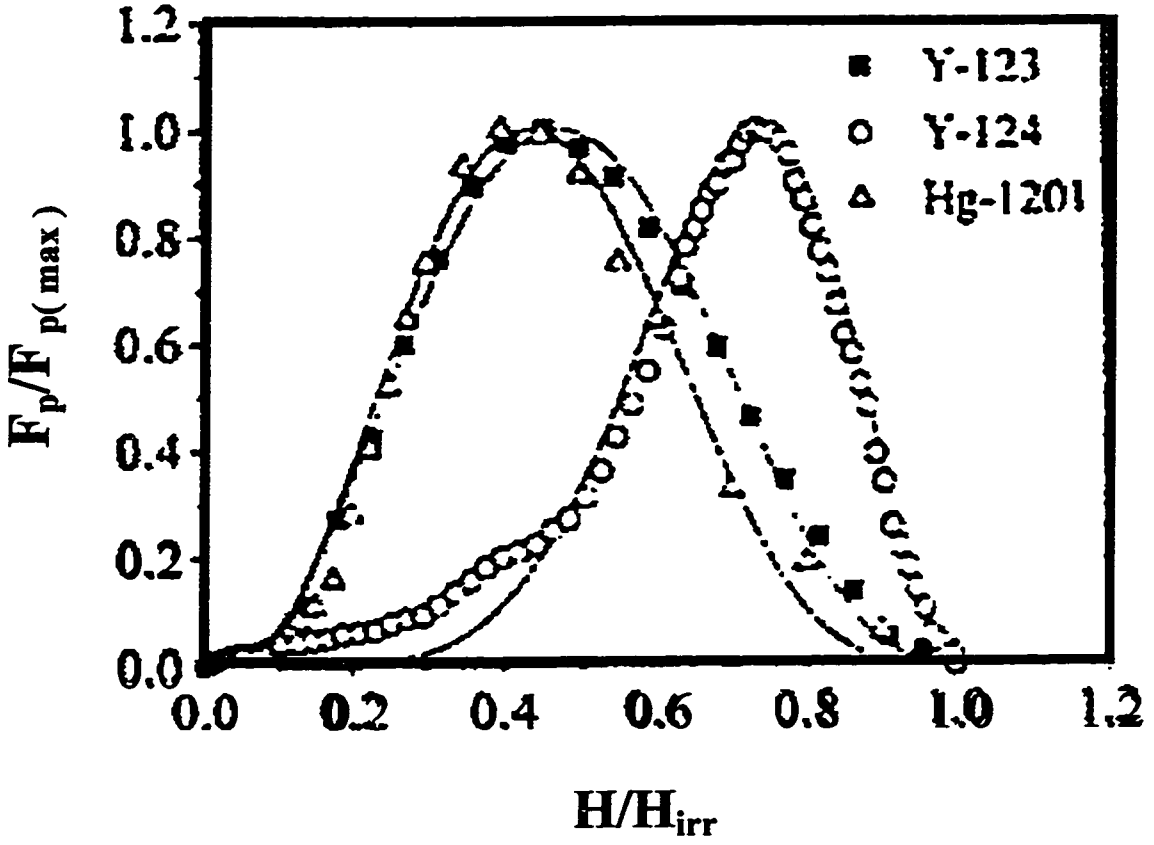

Figure 5.4: The normalizing pinning force $F_p/F_{p(max)}$ as a function of the reduced field H/H_{irr} for Y-123 , Y-124 and Hg-1201 at T around T_c of each sample [41].

5.4.1 Scaling Parameter:

The results presented in figure 5.3, describe the changes in pinning force versus H at different temperatures. The curves start linearly then bend to another linear behavior. There exists threshold fields in these curves that can be determined by the intersection point of the initial linear slope and the high field linear saturation slope. This point is denoted by H_p and represents the threshold field or full penetration field above which the pinning force approaches saturation "or maximum" gradually. The scaling parameter is taken as H_p. Figure 5.5 provides a graphical determination of H_p for ZFC state at a selected temperature, (T=2K). Also shown in the figure the corresponding pinning force $P_f(p)$ at H_p.

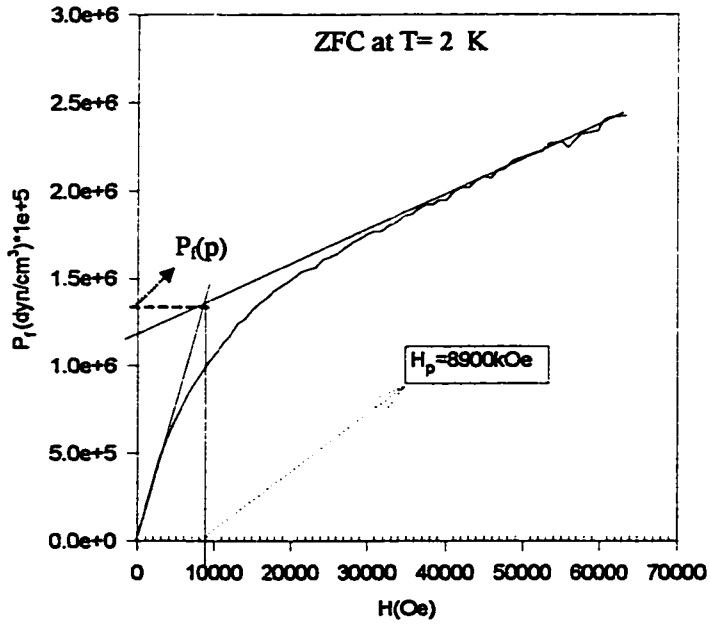

Figure 5.5 : Scaling parameter H_p at T=2 K for ZFC state .

At higher temperatures, H_p (and $P_f(p)$) decreases exponentially according to, $H_p = H_{p0}\, e^{-\alpha T}$, the results are shown in Figure 5.6 for FC and ZFC states. For both states, H_p follows a similar temperature dependence. The parameters H_{p0} and α are listed in table 5.1.

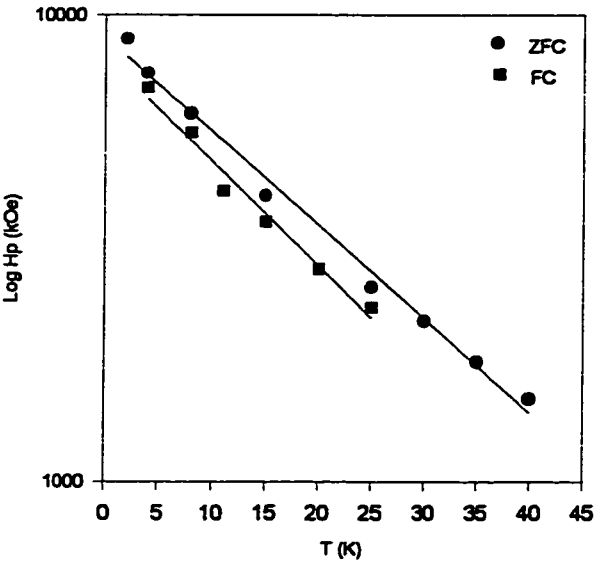

Figure 5.6 : Scaling parameter H_p for FC and ZFC states.

Table 5.1

Fitting parameters for figure 5.6.

	α (1/K)	H_{p0} (kOe)	R^2
ZFC	-0.02	3.95	99%
FC	-0.023	3.91	97.8%

In the following sections we will use this H_p to check the scaling behavior of J_c and P_f.

5.4.2 Scaling of Critical Current Density J_c

In Figures 5.7 and 5.8 we represent the normalized critical current J_n, obtained by: ($\frac{4\pi J_c}{H_p}$), versus H_n for ZFC and FC states, where H_n represents the normalized field H/H_p . Figures 5.7 and 5.8 show almost universal behavior that the scaling is obeyed, since all data point fall in one line. The FC state clearly exhibit universal scaling behavior over a wide range of temperatures. The estimated noise level in normalized critical current J_n is abc

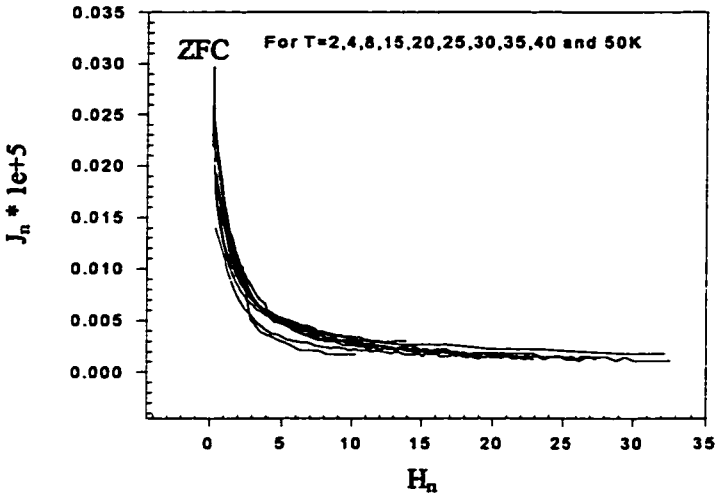

Figure 5.7 : Scaling of J_c for different temperatures for ZFC state.

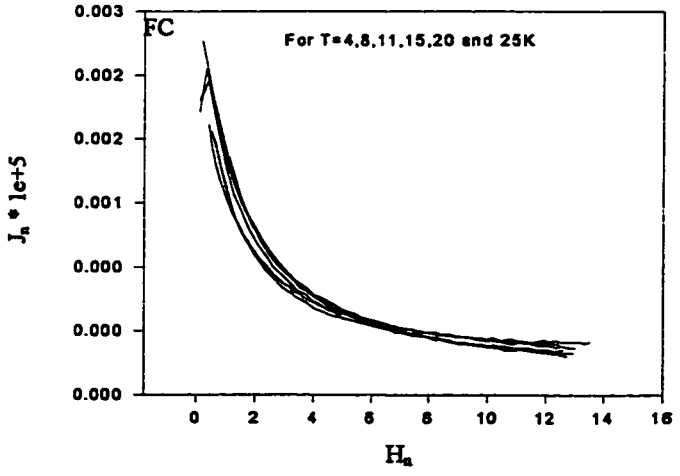

igure 5.8 : Scaling of J_c for different temperatures for FC state.

5.4.3 Scaling of Pinning Force P_f

Figures 5.9 and 5.10 show the normalizing pinning force P_n that is obtained from the formula: ($P_n = \frac{4\pi * p_F}{H^2_p}$), where P_f is an energy per unit volume and also H_p^2 represents the energy required for full penetration field, versus H_n for ZFC and FC states. From figure 5.9 for the ZFC state, the data roughly follows a universal scaling curve that increases linearly (initially) with increasing field H_n, then gradually approach saturation. Similar behavior is followed for the FC state as seen in figure 5.10.

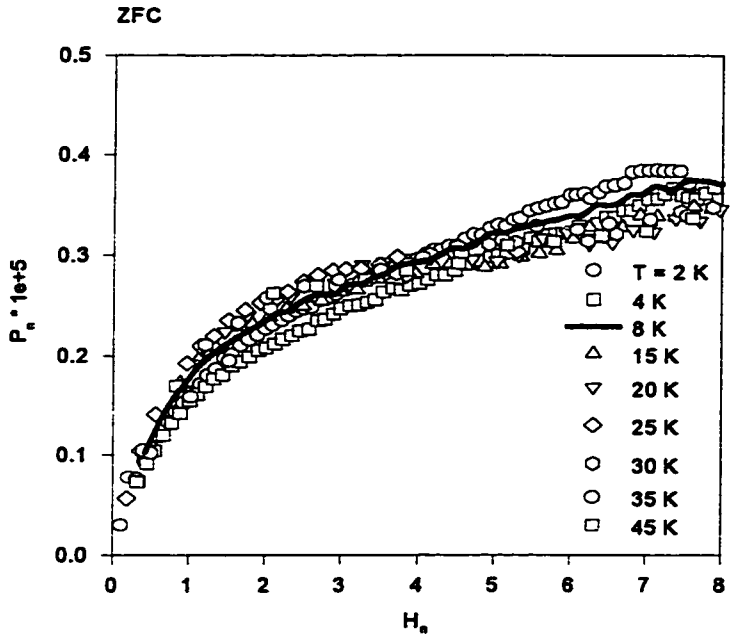

Figure 5.9: Scaling pinning force P_n data for different temperatures for ZFC state.

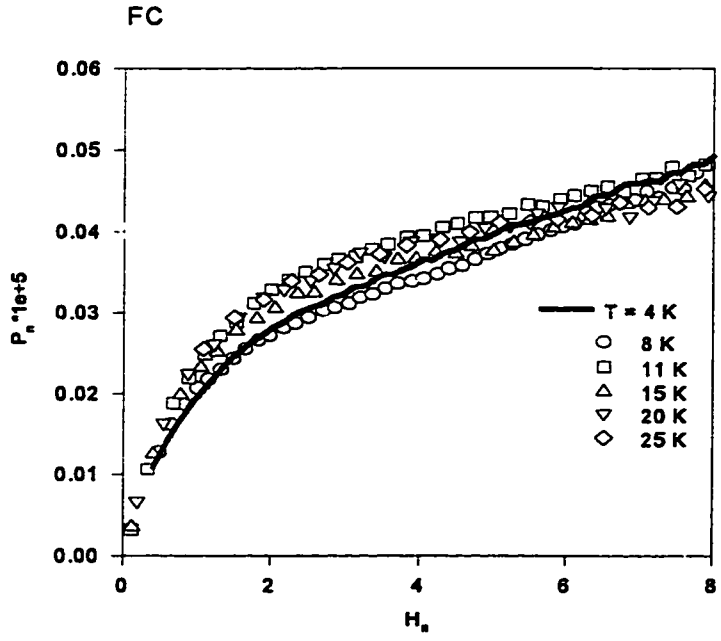

Figure 5.10: Scaling pinning force P_n data for different temperatures for FC state.

5.4.4 Scaling of Hysteresis Loops:

In chapter 3 we adapted a two parameter scaling procedure in scaling the hysteresis loops in different regions of field (low field and high field regions) and different temperatures. That scaling method concentrated on the saturated and non-saturated trapped flux states. The results discussed in chapter 3 showed that the scaling behavior is being obeyed more clearly in the FC state than the corresponding ZFC state, especially for the saturated part of M_r when using two scaling parameters.

In this section, we apply our one parameter scaling method to scale the hysteresis loops. The results are shown in figure 5.11 as normalized magnetization ($4\pi M/H_p$) versus (H/H_p), and they clearly show the lack of scaling behavior. The positive magnetic (normal state) contribution to the hysteresis loop causes the non-scaling behavior. It seems appropriate to subtract the normal state contribution from the hysteresis then normalize the contribution of superconducting state only.

Since at high field the material is in the normal state, by fitting the curve in that region and forcing the fit through zero, the normal state can then be subtracted from the hysteresis loop. After this step the scaling procedure was applied, and the result is shown in figure 5.12. Here we see the scaling criteria is also satisfied for hysteresis loops.

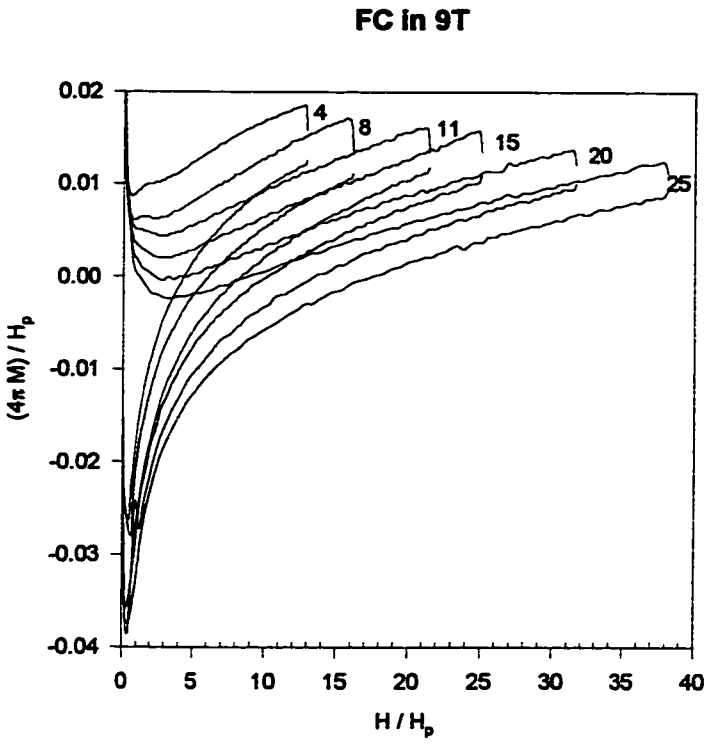

Figure 5.11 : Scaling hysteresis loops, for FC in 90 kOe, including normal state contribution for temperatures 4,8,11,15,20 and 25K.

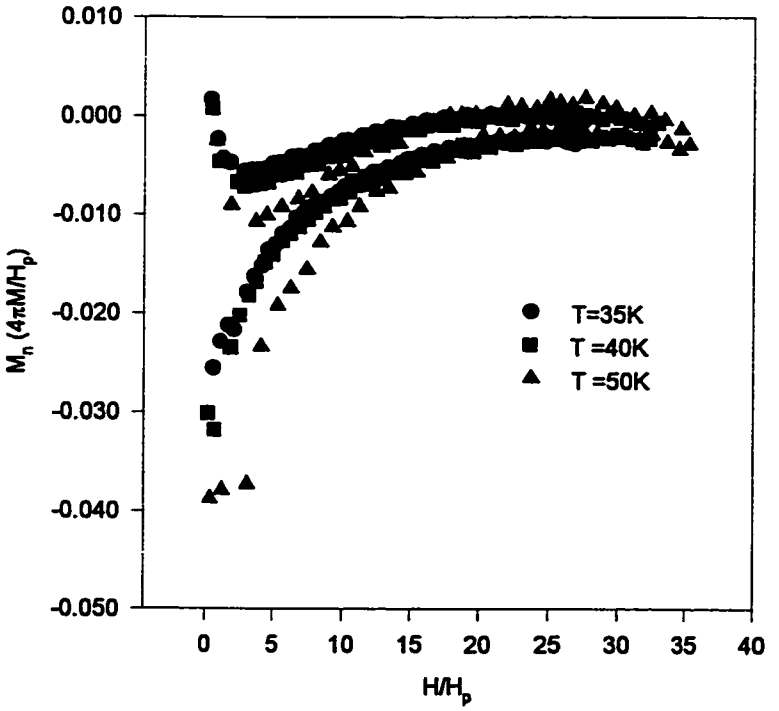

Figure 5.12: Scaling hysteresis loops after normal state correction.

5.5 Conclusion:

Throughout this chapter a one parameter scaling procedure for pinning force (P_f) and critical current (J_c) was successfully applied over a wide temperature range. The scaling behavior is followed for both P_f and J_c over a wide range of temperatures. It is observed that a clearer of universal behavior has been seen for the FC state over the ZFC state. Scaling of the hysteresis loops, after subtracting the normal state contribution from the hysteresis data, also gave a good universal scaling behavior for the same scaling parameter H_p.

CHAPTER 6

Conclusion

Through this work, a polycrystal superconductor sample (Y_{124}) has been prepared to study its magnetic properties like hysteresis loops, remanent magnetization and energy losses. Also further study has been done in order to obtain a reasonable scaling procedure to some superconducting properties of our sample (Y_{124}) such as remanent magnetization, hysteresis loops, energy losses, critical current and pinning force.

Scaling behavior of the remanent magnetization was satisfied over a wide range of temperatures, using two scaling parameters M* (remanent magnetization at saturation) and H* (field at saturation).

Scaling behavior of the hysteresis loops obtained at different temperatures over a wide range of cycling fields for FC and ZFC sates has been followed using two methods. In chapter three, the scaling process was based on using two scaling parameters, H_{max} and M_r. Scaling was satisfactory only for the saturated region, at high field and high temperature. The other method is based on, first subtracting the normal state contribution

from the hysteresis data, then scaling the hysteresis loops using one scaling parameter H_p. This gives a good universal scaling behavior without dividing the hysteresis data into two regions or using two scaling parameters like the analysis performed in chapter three, *see chapter 5 section 5.4.4.*

Energy losses, have also been studied for the FC state and the ZFC state. For Y_{124}, the energy losses decrease when increasing the temperature. While the energy losses increase for increasing the field showing different field dependence than expected from Bean's model. Scaling of energy loss is done for two regions using two scaling parameters, W_{max} and H^*. The results proved that the scaling of the FC state is a better fit than that for the ZFC state, *see chapter 4.*

Finally, a successful scaling procedure was achieved for pinning force P_f and critical current J_c using one scaling parameter H_p. Clear scaling behavior has been seen for the FC and ZFC state, *see chapter 5 sections 5.4.2 and 5.4.3.*

The scaling model was achieved as follows:

Using one scaling parameter, various magnetic properties (P_f, J_c and hysteresis loops) were scaled over a wide range of temperatures.

Further research on other scaling parameters and magnetic properties seems appropriate since H_p may not be unique. It would be interesting to further investigate scaling properties of irreversibility field, and thermodynamic critical field.

Bibliography

1. Rose Innes, A.C., and Rhodrick, E.H., Introduction to Superconductivity, Pergamon Press, Oxford, 1968.

2. Kresin, W., Introduction to Superconductivity, McGraw Hill, New York,1992.

3. Danial, H., Superconductivity Sourcebook, John Wiley & Sons Publications, New York, 1989.

4. Kittle, C., Introduction to Solid State Physics, John Wiley, New York, 1986.

5. Abrikosov, A. A., JETP 5 (1957) 1174.

6. Munson, M., I&M News Letter, issue 126, (1995) 6.

7. Bednorz, J., and Muller, K., Z.Phys.B 64,(1986) 189.

8. Beasley, M.R., Geballe, T.H., Phys.Today 36 (10), (1984) 60.

9. Chu, G., Wu, M., Ashburn, J.,Torng, C., Hor, P., Meg, R., Gao, L., Haung, Z., and Wang, Y., Phys.Rev.Lett.58, (1987) 908.

10. Maeda, H., Tanaka, Y., Fukutomi, M., and Asona, T., Jpn.J.Appl.Phys.27 (1988) L207.

11. Numata, K., Mori, K., Yamamota, H., Inoue, K., and Maeda, H., J.Appl.Phy.64, (1988) 11.

12. Ginsberg, D., Physical Properties of High Temperature Superconductors I, World Scientific, 1989.

13. Schlling, A., Antipov, E. V., Marezio, M., Nature 363 (1993) 50.

14. Burns, G., High Temperature Superconductivity, AP. Inc.,1991.

15. Malozemoff, A., Phy.Rev.B 38(10) (1988) 6490.

16. Kramer, E., J.Appl.Phys.44, (3) (1973) 1360.

17. Juang, J., Wang, S., Uen, T., and Gou, Y., Phy. Rev. B 46(2) (1992) 1188.

18. Chang, J., Claire, S., Jurgen, S., and Brend, S., Phys. Rev. B 48 (1993) 13911.

19. Wei, C.D., Liu, Z.X., and Gan, Z.Z., Phys. C 195 (1992) 286.

20. Song, L.W., Yang, M., Chen, E., and Kao, Y.H., Phy. Rev. B 45(6) (1992) 3083.

21. Wollfus, Y., Yeshurun, Y., Felner, I., and Sompolinsky, H., Phys.Rev.B 40, (1989) 2701.

22. Hans Ullmaier, Irreversible Properties of Type II Superconductors, Springer-Verlag (1975).

23. Pramana, A., Ms. Thesis, KFUPM, Phy.Dept., (1995) unpublished.

24. Senoussi, S., J.Phys.III (Paris)2, (1992) 10411.

25. Carr, W., AC Loss and Macroscopic Theory of Superconductors, Gordon and Breach, New York, 1983.

26. Doverspike, K., Hubbard. C.R., Williams, R.K., Alexander, K.B., Brynestad, J., and Kroeger, D.M., Phys. C 172 (1991) 486.

27. Trofimov, V. N., Kuznetsov, A. V., Sinchenko, A. A., Bolschinskov, K. A., and Ivanov, A. A., Phys. B 194-196 (1994) 2327.

28. Wei, C. D., Liu, Z. X., Gan, Z. Z., Ren, H. T., Xiao, L., and He, O., Phys. C 241 (1995) 83.

29. Bean, R. P., Rev.Mod.Phys.36 (1964) 31.

30. Kim, S. F., Labdi, S., Li, Z. Z., and Raffy, H., Phys. C 235-240 (1994) 2843.

31. Job, R., and Rosenberg, M., Phys. C 172 (1991) 391.

32. Wei, C. D., Liu, Z. X., and Gan, Z. Z., Phys. C 222 (1994) 267.

33. Muller, K., IEEE Trans.Mag., 27 no.(2), March (1991) 2174.

34. Muller, K., and Pauza, A., Phys. C 161 (1989) 319.

35. Clem, J. R., Physica C 153-155 (1988) 50.

36. Kwasnitza, K., At.Clerc, Phys. C 233 (1994) 423.

37. Huebner, R. P., Magnetic Flux Structure in Superconductors, Springer-Verlag (1979).

38. Ziq, Kh.A., Hamdan, N.M., and Al- Harthi, A.S., in "Advances in Superconductivity X", ed. K. Osamura and I. Hirabayashi, Proceedings of the 10th International Symposium on Superconductivity (ISS97), October 27-30,1997 Gifu-Japan, page 585.

39. Pramana DN, A.A., Ziq, Kh.A.,and Hamdan, N.M., Phys. C 282-287 (1997) 1445.

40. Livingston, J.P., Rev. Mod.Phys. 36 no.(1),part(1), (1964) 54.

41. Wisniewski, A., Puzniak, R., Szymczak, R., Baran, M., and Karpinski, J., J.M.M.M. 177-181 (1998) 499.

42. Clem, J.R., in "Advances in Superconductivity X", ", ed. K. Osamura and I. Hirabayashi, Proceedings of the 10th International Symposium on Superconductivity (ISS97), October 27-30,1997 Gifu-Japan, page 23.

43. See for example M.R. Koblischka, et al. in "Advances in Superconductivity X", ", ed. K. Osamura and I. Hirabayashi, Proceedings of the 10th International Symposium on Superconductivity (ISS97), October 27-30,1997 Gifu-Japan, page 517.

IMAGE EVALUATION
TEST TARGET (QA-3)

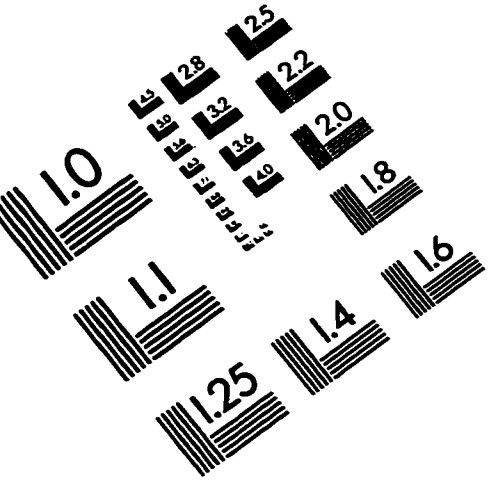

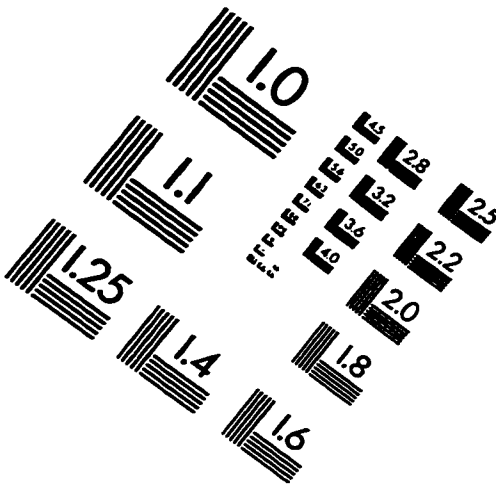

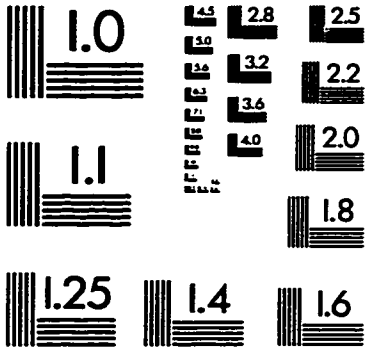

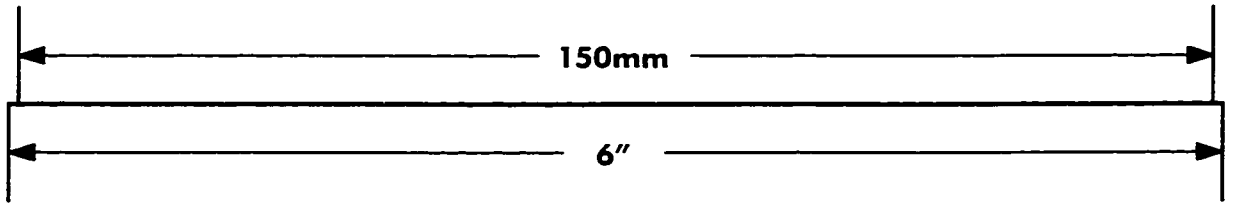

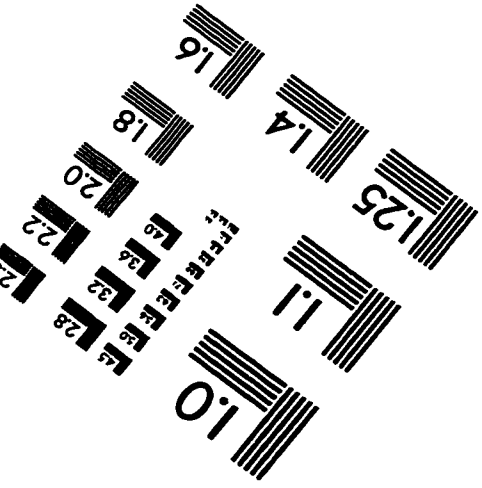

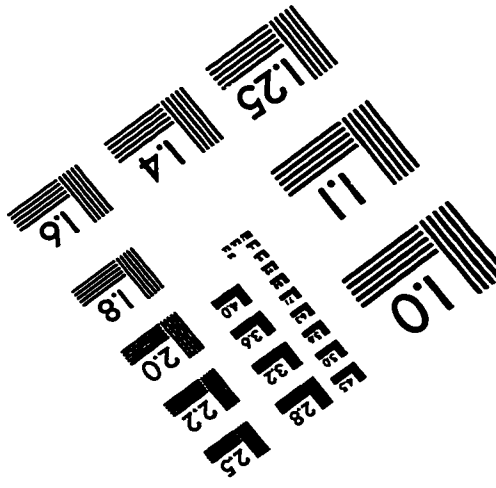

APPLIED IMAGE, Inc
1653 East Main Street
Rochester, NY 14609 USA
Phone: 716/482-0300
Fax: 716/288-5989